Drilling constraints on lithospheric accretion and evolution at Atlantis Massif, Mid-Atlantic Ridge 30°N

D. K. Blackman,[1] B. Ildefonse,[2] B. E. John,[3] Y. Ohara,[4] D. J. Miller,[5] N. Abe,[6] M. Abratis,[7] E. S. Andal,[8] M. Andreani,[9] S. Awaji,[10] J. S. Beard,[11] D. Brunelli,[12] A. B. Charney,[13] D. M. Christie,[14] J. Collins,[15] A. G. Delacour,[16] H. Delius,[17] M. Drouin,[18] F. Einaudi,[2] J. Escartín,[19] B. R. Frost,[3] G. Früh-Green,[20] P. B. Fryer,[21] J. S. Gee,[1] M. Godard,[2] C. B. Grimes,[22] A. Halfpenny,[23] H.-E. Hansen,[24] A. C. Harris,[25] A. Tamura,[26] N. W. Hayman,[27] E. Hellebrand,[21] T. Hirose,[28] J. G. Hirth,[29] S. Ishimaru,[26] K. T. M. Johnson,[21] G. D. Karner,[30] M. Linek,[31] C. J. MacLeod,[32] J. Maeda,[33] O. U. Mason,[34] A. M. McCaig,[35] K. Michibayashi,[36] A. Morris,[37] T. Nakagawa,[38] T. Nozaka,[39] M. Rosner,[40] R. C. Searle,[41] G. Suhr,[42] M. Tominaga,[15] A. von der Handt,[43] T. Yamasaki,[33] and X. Zhao[44]

Received 13 August 2010; revised 9 February 2011; accepted 25 April 2011; published 19 July 2011.

[1] Expeditions 304 and 305 of the Integrated Ocean Drilling Program cored and logged a 1.4 km section of the domal core of Atlantis Massif. Postdrilling research results summarized here constrain the structure and lithology of the Central Dome of this oceanic core complex. The dominantly gabbroic sequence recovered contrasts with predrilling predictions; application of the ground truth in subsequent geophysical processing has

[1]Scripps Institution of Oceanography, University of California, San Diego, La Jolla, California, USA.
[2]Géosciences Department, Université Montpellier 2, Montpellier, France.
[3]Department of Geology and Geophysics, University of Wyoming, Laramie, Wyoming, USA.
[4]Hydrographic and Oceanographic Department, Ocean Research Laboratory, Tokyo, Japan.
[5]Integrated Ocean Drilling Program, Texas A&M University, College Station, Texas, USA.
[6]IFREE, JAMSTEC, Yokosuka, Japan.
[7]Institute of Geosciences-Mineralogy, Friedrich Schiller University of Jena, Jena, Germany.
[8]Philex Mining Corporation, Pasig City, Philippines.
[9]Laboratoire de Géologie, Université Claude Bernard Lyon 1, Villeurbanne, France.
[10]Department of Geosystem Engineering, University of Tokyo, Tokyo, Japan.
[11]Virginia Museum of Natural History, Martinsville, Virginia, USA.
[12]Dipartimento di Scienze della Terra, Universita Modena, Modena, Italy.
[13]Department of Geosciences, Oregon State University, Corvalis, Oregon, USA.
[14]Department of Fisheries and Ocean Sciences, University of Alaska Fairbanks, Fairbanks, Alaska, USA.
[15]Department of Marine Geology and Geophysics, Woods Hole Oceanographic Institution, Woods Hole, Massachusetts, USA.
[16]Laboratoire de Dynamique Terrestre Planétaire, Université Toulouse, Toulouse, France.
[17]Department of Geology, University of Leicester, Leicester, UK.
[18]Laboratoire Geosciences, Université Réunion, Saint-Denis, France.
[19]Groupe de Geosciences Marines, Institut de Physique du Globe, Paris, France.
[20]Department of Earth Sciences, ETH Zurich, Zurich, Switzerland.
[21]School of Ocean and Earth Science and Technology, University of Hawaii at Manoa, Honolulu, Hawaii, USA.
[22]Department of Geosciences, Mississippi State University, Mississippi State, Mississippi, USA.
[23]Research School of Earth Sciences, Australian National University, Canberra, ACT, Australia.
[24]Department of Earth Science, University of Bergen, Bergen, Norway.
[25]Department of Geology and Environmental Sciences, Norwich University, Northfield, Vermont, USA.
[26]Department of Earth and Environmental Sciences, Kanazawa University, Kanazawa, Japan.
[27]Institute of Geophysics, University of Texas at Austin, Austin, Texas, USA.
[28]Kochi Institute for Core Sample Research, JAMSTEC, Nankoku City, Japan.
[29]Department of Geological Sciences, Brown University, Providence, Rhode Island, USA.
[30]Exxon-Mobile URC, Houston, Texas, USA.
[31]Baker Hughes, Houston, Texas, USA.
[32]Department of Earth and Ocean Sciences, Cardiff University, Cardiff, UK.
[33]Department of Earth and Planetary Sciences, Hokkaido University, Sapporo, Japan.
[34]Ecology Department, Lawrence Berkeley National Laboratory, Berkeley, California, USA.
[35]Department of Earth Sciences, University of Leeds, Leeds, UK.
[36]Institute of Geosciences, Shizuoka University, Shizuoka, Japan.
[37]Department of Earth and Environmental Sciences, University of Plymouth, Plymouth, UK.
[38]Department of Chemical and Life Sciences, Nihon University, Fujisawa, Japan.
[39]Department of Earth Sciences, Okayama University, Okayama, Japan.
[40]Mineral Properties and Transport Processes, GFZ, Potsdam, Germany.
[41]Department of Earth Sciences, Durham University, Durham, UK.
[42]Institut für Geologie und Mineralogie, Universitat zu Köln, Cologne, Germany.
[43]Department of Geosciences, University of Freiburg, Freiburg, Germany.
[44]Department of Earth Sciences, University of California, Santa Cruz, California, USA.

0148-0227/11/2010JB007931

produced self-consistent models for the Central Dome. The presence of many thin interfingered petrologic units indicates that the intrusions forming the domal core were emplaced over a minimum of 100–220 kyr, and not as a single magma pulse. Isotopic and mineralogical alteration is intense in the upper 100 m but decreases in intensity with depth. Below 800 m, alteration is restricted to narrow zones surrounding faults, veins, igneous contacts, and to an interval of locally intense serpentinization in olivine-rich troctolite. Hydration of the lithosphere occurred over the complete range of temperature conditions from granulite to zeolite facies, but was predominantly in the amphibolite and greenschist range. Deformation of the sequence was remarkably localized, despite paleomagnetic indications that the dome has undergone at least 45° rotation, presumably during unroofing via detachment faulting. Both the deformation pattern and the lithology contrast with what is known from seafloor studies on the adjacent Southern Ridge of the massif. There, the detachment capping the domal core deformed a 100 m thick zone and serpentinized peridotite comprises ~70% of recovered samples. We develop a working model of the evolution of Atlantis Massif over the past 2 Myr, outlining several stages that could explain the observed similarities and differences between the Central Dome and the Southern Ridge.

Citation: Blackman, D. K., et al. (2011), Drilling constraints on lithospheric accretion and evolution at Atlantis Massif, Mid-Atlantic Ridge 30°N, *J. Geophys. Res.*, *116*, B07103, doi:10.1029/2010JB007931.

1. Introduction

[2] Deep drilling of the domal core of Atlantis Massif, Mid-Atlantic Ridge 30°N (Figure 1), has provided insights into the formation of slow spread lithosphere, and constraints on the structure and evolution of oceanic core complexes (OCC) that could not have been obtained from seafloor mapping and sampling alone. The information obtained by coring and borehole logging were a key motivation for increasing the sophistication of regional geophysical analyses, which, in turn, advanced interpretations of the subsurface structure. Integrated Ocean Drilling Program (IODP) Expeditions 304–305 drilling results [*Blackman et al.*, 2006] provided first-order information that the Central Dome is composed of dominantly gabbroic rocks, in contrast to early geological and geophysical interpretation that predicted this region to be underlain by ultramafic rocks. Postexpedition investigations have targeted a variety of more complex questions. In this paper we summarize many of the postcruise results and compare these to results from seafloor studies on the southern part of the domal core, the Southern Ridge (Figure 1a). We proceed with new analyses, discussing the implications in terms of the formation and evolution of the whole core complex.

[3] Slow spread ocean lithosphere accretes and evolves via temporally and spatially variable magmatic and tectonic processes [e.g., *Bonatti and Honnorez*, 1976; *Karson et al.*, 1984; *Dick*, 1989; *Lin et al.*, 1990; *Sinton and Detrick*, 1992; *Cannat*, 1993; *Lagabrielle et al.*, 1998]. OCCs, in particular, mark significant periods (1–2 Myr) where a distinct mode of rifting/accretion persists, in contrast to the more typical interplay between magma supply and faulting that generates the ubiquitous abyssal hills. Long-lived displacement along detachments active within the ~20 km wide axial zone of a spreading center exhume the characteristic domal cores of an OCC, often capped by spreading-parallel corrugations [e.g., *Cann et al.*, 1997; *Tucholke et al.*, 1998]. Beneath this exposed fault zone, gabbroic rocks with lenses, and possibly more significant volumes of mantle peridotite are present, providing access to a major component of Earth's deep lithosphere for detailed chemical and physical property investigations. Conditions of OCC development are documented by igneous and metamorphic assemblages, as well as by deformation recorded during evolution of the footwall.

[4] Atlantis Massif is a young OCC where contextual data from regional geophysical surveys, as well as seafloor mapping and sampling is good, and major structural blocks within the faulted lithosphere have been identified (Figure 1). Drilling targeted the Central Dome while a majority of the seafloor studies have taken advantage of outcrops accessible on the steep face of the Southern Ridge, the 'South Wall' (Figure 2), where the dome plunges toward the transform valley. In the final section of this paper, we consider results for both of these parts of Atlantis Massif, and we develop a model for the formation and evolution of the whole OCC.

[5] Some initial inferences based on predrilling and/or shipboard analysis [*Blackman et al.*, 2006] have been superseded by new interpretations that incorporate in-depth postcruise results, as discussed in the following sections. These updates include: consistency of geophysical models of the Central Dome of Atlantis Massif; the age of crust drilled (and associated plate spreading rate during core complex formation); the genesis of recovered olivine-rich troctolite; the nature of metamorphism; and systematic tectonic rotation of the footwall based on paleomagnetic data.

2. Geologic Setting

[6] Sea surface magnetic anomalies indicate that the lithosphere comprising Atlantis Massif is between 0.5 and 2 Ma. Average plate spreading rate over the past ~5 m.y. has been ~24 mm/yr (full rate) [*Pariso et al.*, 1996]. Atlantis Massif was initially hypothesized to be an OCC on the basis of morphologic and backscatter mapping, and dredging results that documented the shallow, corrugated and striated domal core underlain by mafic and ultramafic rocks [*Cann et al.*, 1997]. The spreading-parallel corrugations are equated with similar-scale features mapped on continental detachment faults

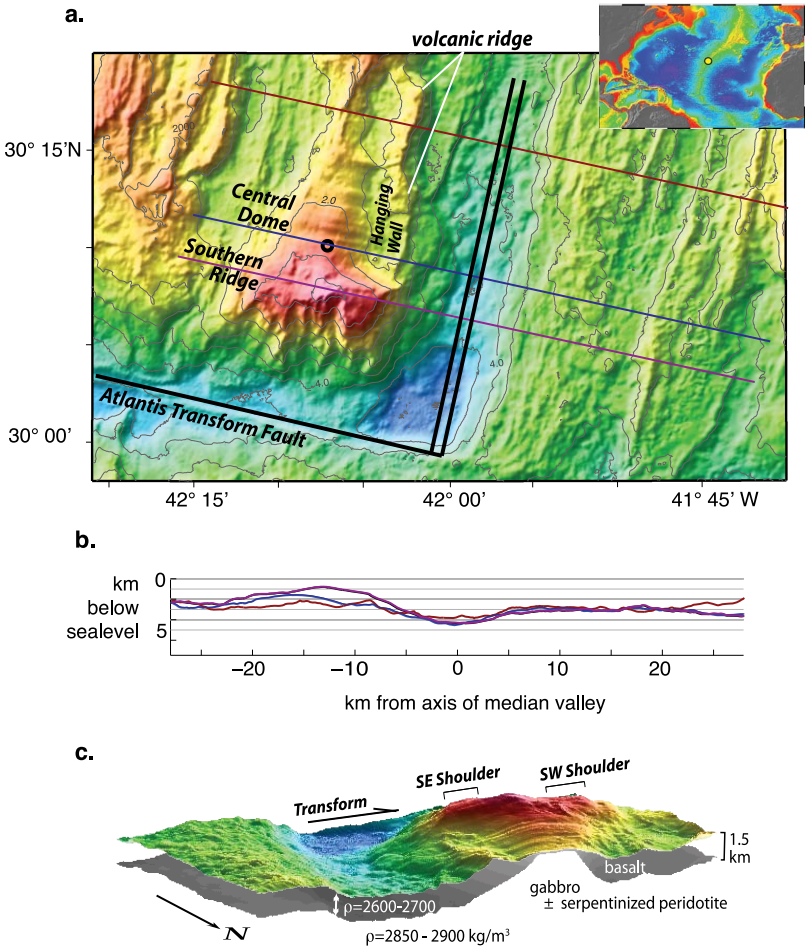

Figure 1. Seafloor topography in the vicinity of the intersection of the Mid-Atlantic Ridge and Atlantis transform fault and basic structure of Atlantis Massif oceanic core complex. (a) Contour interval 0.5 km. Corrugated surface is inferred to be exposed detachment capping the domal high. Axis of the Mid-Atlantic Ridge and Atlantis Transform Fault are shown by black lines; circle marks IODP Site U1309. Location of profiles across the middle of the segment (brown), the Central Dome (blue) and the Southern Ridge (purple) are shown. (b) Seafloor depth along these three profiles. (c) Perspective view of Atlantis Massif looking SSW. Gray interface shows 3-D model of upper/lower crustal boundary that can explain most of the Bouguer gravity anomaly in this area.

[*John*, 1987], and suggest it was a slip surface associated with the detachment fault that unroofed the dome. *Schroeder and John* [2004] and *Karson et al.* [2006] document deformation within a zone that confirms the existence of a long-lived normal fault at the top of at least parts of the Southern Ridge. The juxtaposition of volcanic eastern blocks against the corrugated dome, where southern ridge samples include gabbroic rocks and serpentinized peridotite, supports the OCC model (Figure 2). Gravity and seismic data indicate that significant portions of the footwall to the detachment contain rocks with anomalously high density (200–400 kg/m^3 greater than surrounding rock) [*Blackman et al.*, 1998; *Nooner et al.*, 2003], and velocities (4–6 km/s in the upper km, compared to average Atlantic upper crust at ~3–5 km/s) [*Canales et al.*, 2008; *Collins et al.*, 2009].

[7] The development of this OCC at the eastern intersection of the Mid-Atlantic Ridge (MAR) with the Atlantis fracture zone is just one of three instances over the past ~9 m.y. where an OCC is inferred to have formed at one of the inside corners in this area [*Cann et al.*, 1997]. Both the older OCCs shoal to 1000 m, somewhat deeper than the peak of Atlantis Massif [*Blackman et al.*, 1998, 2002] but similar to the average depth of the Southern Ridge (Figure 1b). The active serpentinite-hosted Lost City hydrothermal vent field [*Kelley et al.*, 2001; *Früh-Green et al.*, 2003] is located just below the peak of the massif, the apex of the Southern Ridge. The Central Dome extending smoothly to the north is several hundred meters deeper, and it is against only this part of the footwall that the juxtaposed volcanic hanging wall exists. It is assumed to overly the detachment where it extends at depth. The existence of large throw normal faults toward the median valley likely indicates that major slip along the detachment has ceased [e.g., *Cannat et al.*, 2009].

[8] Mapping and sampling along the Southern Ridge of Atlantis Massif (Figure 2) shows that detachment processes in that area were concentrated in a zone about 100 m thick [*Schroeder and John*, 2004] and that the fault is continuous for at least a few km in the spreading direction [*Karson*

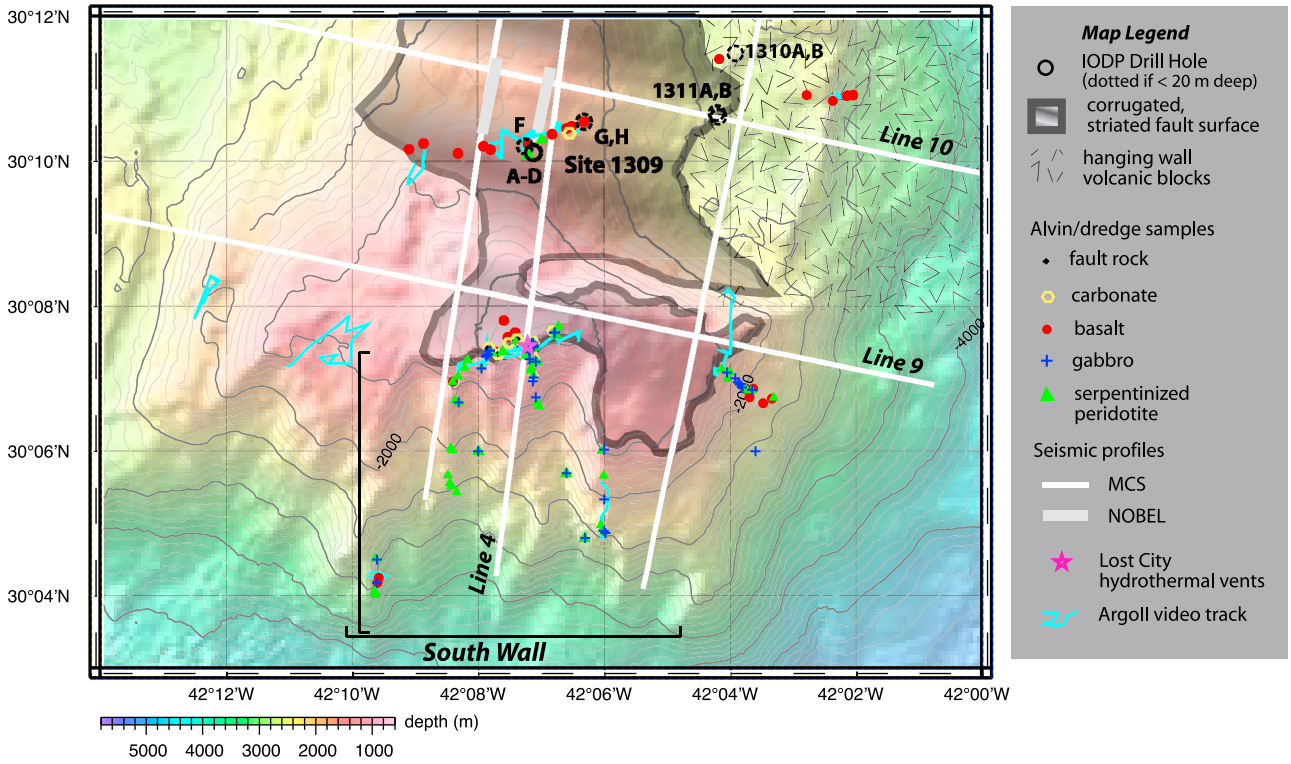

Figure 2. Geologic data and selected geophysical tracks at Atlantis Massif. Sonar coverage is complete at 100 m scale as is side scan at 10 m scale. The latter delineates extent of striations that parallel corrugations on the exposed detachment fault that caps the domal core comprising the footwall of the OCC. The volcanic hanging wall juxtaposed east of the Central Dome flanks the median valley of the spreading axis. Majority of rock sample symbols indicate collection by submersible, as indicted by close spacing along relatively continuous paths. MCS, multichannel seismic line; NOBEL, near bottom seismic source shooting line with seafloor seismographs located at each end.

et al., 2006]. Thin carbonate sediment in many places is lithified and covers much of the detachment on top of the domal core, impeding direct mapping and sampling of fault surface [*Blackman et al.*, 2002]. Below the carbonate interval, less than 1 m thick, a breccia unit 1–3 m thick has been mapped locally, unconformably overlying the detachment shear zone [*Karson et al.*, 2006]. Basaltic rubble was mapped and sampled along a transect across the Central Dome, and the alteration minerals in these samples (chlorite, amphibole and later clays) indicate metamorphism at temperatures too high for near-seafloor conditions. *Blackman et al.* [2002] inferred this to indicate they are probably remnants from the base of the hanging wall after its displacement along the detachment fault. Additional aspects of the Southern Ridge geology and geophysics are discussed in Section 7; we focus the next several sections on the drilling results for the Central Dome.

3. Drilling Strategy and Gabbroic Sequence Recovery

[9] Determining the processes that operate during formation of OCCs was the overriding goal of drilling at Atlantis Massif [*Blackman et al.*, 2004]. In addition, the potential for recovery of unaltered ultramafic rock, suggested to be present at depths as shallow as several hundred meters subseafloor based on initial seismic analyses [*Canales et al.*, 2004; *Collins et al.*, 2003], generated significant interest in the community. The drilling plan for IODP Expeditions 304 and 305 was designed to address questions about the proposed detachment zone itself, the footwall, and geochemical and structural relationships between the domal core and the volcanic hanging wall (Table 1) [*Blackman et al.*, 2004].

[10] Attempts to start a reentry hole in the western part of the hanging wall (IODP Sites U1310 and U1311; Figure 2) were unsuccessful; no samples were obtained from an

Table 1. Hypotheses Targeted by IODP Expeditions 304 and 305

Hypothesis	Description
1	A major detachment fault system controlled the evolution of Atlantis Massif.
2	Plate flexure (rolling hinge model) was the dominant mechanism of footwall uplift.
3	Significant unroofing occurred during formation of this OCC.
4	The nature of melting &/or magma supply contributed to episodes of long-lived lithospheric faulting.
5	Expansion associated with serpentinization contributed significantly to uplift of the domal core.
6	The Mohorovicic discontinuity (Moho) at Atlantis Massif is a hydration front.
7	Positive gravity anomalies at Atlantis Massif indicate relatively fresh peridotite.

unexposed section of the detachment, hypothesized to underlie this block [*Canales et al.*, 2004]. Minimal recovery from the upper ~10 m of the hanging wall obtained relatively fresh basalt, but the samples are insufficient for detailed structural or petrologic studies.

[11] In contrast, drilling conditions on the Central Dome at IODP Site U1309 (Figure 2) were excellent. A pilot hole (U1309B) was drilled to bit destruction, core was recovered throughout the 101 m deep section, and the hole logged. Following an aborted attempt to establish a reentry hole (U1309C), Hole U1309D was established 20 m to the north of Hole U1309B and penetrated to 1415 mbsf, over a series of alternating coring and logging runs. A combination of instrument problems and poor weather precluded the final seismic logging run. Therefore, only the upper 800 m of the formation have this coverage, but other borehole measurements were obtained throughout the >1400 m hole. The hole was in good condition at the end of Expedition 305 and our expectation is that it remains open and could be reentered should future logging, monitoring, or drilling efforts be pursued.

[12] The location of Holes U1309B and D reflected a variety of factors. The smoothness and scale of the domal core were inferred to indicate homogeneous properties (composition, deformation, alteration) over large areas; supporting this inference were the continuity and pervasiveness of a strong seismic reflection 0.2–0.5 s two-way travel time beneath the seafloor, underlying both the Southern Ridge and the Central Dome [*Canales et al.*, 2004]. The drill site was thus selected avoiding fields of rubble known to be present on the dome [*Blackman et al.*, 2002]. Based on preexisting seafloor mapping data showing a rubble free zone near (~400 m), but not exactly on, multichannel seismic profiles, Site U1309 was located in the southern Central Dome. The site is at the southern end of the eastern Near Ocean Bottom Explosive Launcher (NOBEL) refraction line (Figure 2) and along a longer, traditional refraction line.

[13] The ~1.4 km sequence recovered at Site U1309 was dominantly gabbroic, only a few percent of the drill core consisted of ultramafic rock [*Blackman et al.*, 2006]. Recovery was high, averaging ~75% below the uppermost few tens of meters that were either cased (Hole U1309D) or typical low return for the initiation of a deep hole in hard rock (Hole U1309B). The high recovery and subsequent integration of borehole logs with the cores indicate that these samples adequately represent the in situ section. The thick mafic section recovered was key in shifting the original paradigm that detachment faulting and OCC development occur because a portion of the spreading center rifts without significant magmatic input [e.g., *Karson*, 1990; *Tucholke and Lin*, 1994]. Drill and dredge data from other corrugated core complexes [*Dick et al.*, 2000; *MacLeod et al.*, 2002; *Escartín et al.*, 2003; *Kelemen et al.*, 2007], together with work at the (uncorrugated, but likely detachment controlled) Kane inside corner high [*Karson et al.*, 1997], had already indicated that there was magmatic activity during OCC development, but the volume percent was often (although not always) [*Karson and Elthon*, 1987] considered to be low. Three recent models propose that an increase in local magmatism plays an important role in the development of core complexes and that OCCs do not represent the magma-starved end-member of slow-spreading ridges. *Ildefonse et al.* [2007a] suggest that increased local magmatism plays a role in establishment of long-lived detachment faulting. *Tucholke et al.* [2008] use numerical models to predict that increased axial magmatism triggers a shift in faulting away from the active detachment, thus ending OCC development. *MacLeod et al.* [2009] propose that a final stage in the cycle of OCC formation is along-strike propagation of a magmatically robust axial volcanic ridge, which cuts through the detachment, relieves stress and thus ends the long-term activity of the fault.

[14] A secondary goal during Expedition 304 was to obtain samples of the uppermost few meters of the corrugated dome, with the aim of sampling fault rock from the principal slip surface and damage zone associated with the inferred detachment at the seafloor. The *JOIDES Resolution*, with the drill tools onboard at the time, was understood to be less than ideal, but both the principal slip surface and overlying sediment were valuable, so effort was expended for this task on Expedition 304, after progress in Hole U1309D exceeded expectations. This series of shallow holes U1309A, and E-H ranged from 1 to 4 m penetration below seafloor. Recovery of basement rock was less than a few percent of the apparent cored interval. Drilling-disrupted fossiliferous ooze (0–2.5 m) was recovered at Holes U1309A, E, F and G. Holes U1309F, G, and H also included fragments of metabasalt, hyaloclastite, fractured diabase or fragments of talc schist inferred to be fault rock. Similar chromite-bearing talc-tremolite-chlorite schist fragments were found in the uppermost part of the deeper holes, as a clast in a fault breccia at 20 mbsf in Hole 1309B, and as a 10 cm cored interval at 23 mbsf in Hole 1309D. The same assemblages are found in veins replacing ultramafic horizons in the upper 300 m of the core. These rock types are identical to samples obtained within well-mapped seafloor detachment shear zones (15°45′N MAR [*MacLeod et al.*, 2002; *Escartín et al.*, 2003]; the Southern Ridge of Atlantis Massif, [*Boschi et al.*, 2006]), but are absent in the rest of the recovered sequence at Site U1309. Thus, it is likely that they represent samples from a detachment fault, but our recovery falls short of providing irrefutable evidence for (or against) a major shear zone at the seafloor on the Central Dome. The upper 80 m of Holes 1309B and D contain fault breccias composed of basaltic clasts with a green amphibole-rich matrix, and zones of intensely fractured gabbro. They are cut by undeformed but strongly altered basalt and diabase intrusions which comprise about 40% of the recovered core in this interval [*Blackman et al.*, 2006]. These fault breccias and fractured gabbros may be the expression within the gabbro of the well-developed shear zone in serpentinite described from the Southern Ridge of the massif [*Karson et al.*, 2006].

4. Incorporation of the New Constraints in Revised Geophysical Analyses

[15] This section reconciles recovery of a dominantly gabbroic sequence with the predrilling predictions that the dome was underlain mostly by ultramafic rocks, with the potential for fresh peridotite at a shallow depth. Several factors led to initial preference for a model where Atlantis Massif had a core that was dominantly ultramafic. Mapping along the south wall, thought to provide a cross section through the domal core, produced a high percentage of ser-

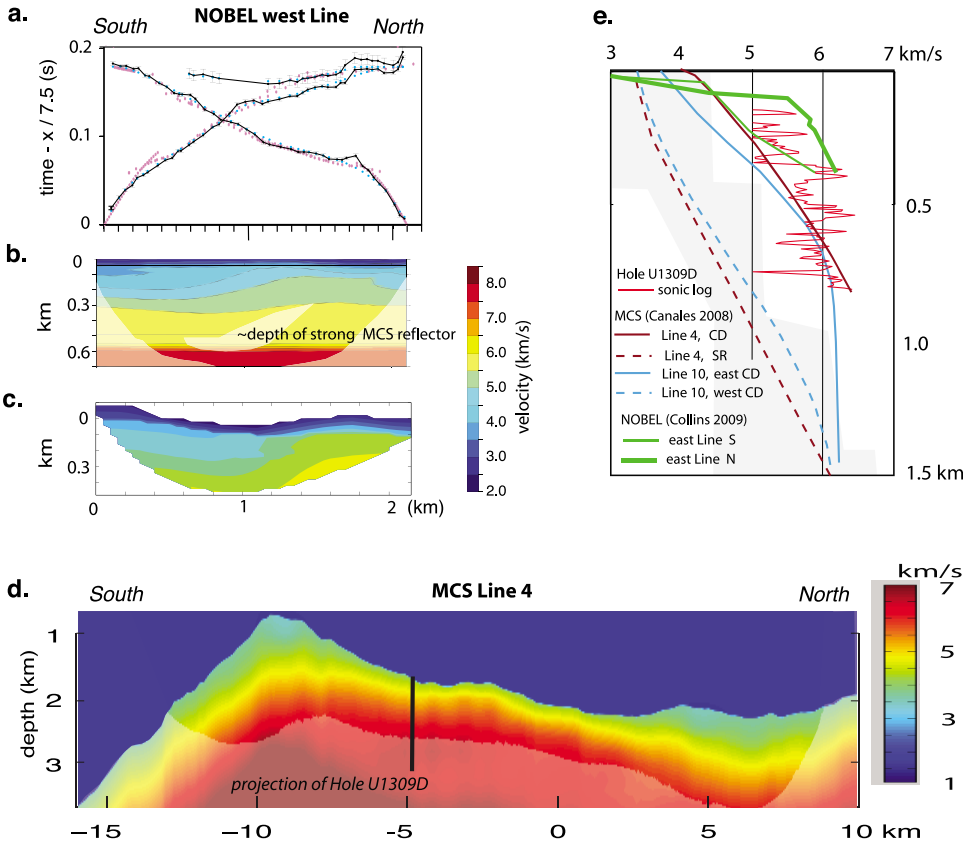

Figure 3. Seismic refraction results. Figures 3a–3c show western NOBEL line on the Central Dome (location in Figure 2): (a) traveltime picks (black) and predicted travel times (cyan) for model in Figure 3b; pink for model in Figure 3c. (b) Velocity model based on inversion of *Collins et al.* [2003]. Areas with no ray coverage are semiopaque. (c) Preferred velocity model determined from forward modeling by *Collins et al.* [2009]. Seafloor topography is included here, unlike in Figure 3b. While this traveltime effect, alone, does not preclude the presence of >7.5 km/s layer, other data do rule one out at shallow depths. (d) Velocity model based on inversion of MCS refractions for Line 4 by *Canales et al.* [2008]. Both color scale and vertical exaggeration differ from that used for Figures 3b and 3c. Area in d not constrained by raypaths is semiopaque. (e) Selected velocity depth profiles illustrate variability within/between structural blocks; light gray region indicates range of typical young Atlantic crustal profiles [*White et al.*, 1992].

pentinized mantle peridotite samples (~70%); gabbro makes up a majority of the remaining sample suite [*Blackman et al.*, 2002; *Boschi et al.*, 2006]. Second, a tomographic inversion fit the NOBEL data well when the top of a >7.5 km/s layer was modeled at 600 mbsf (Figures 3a–3b) [*Collins et al.*, 2003]. This shallow, sharp transition to high velocity was consistent with interpretation of the multichannel seismic (MCS) reflection results, where a strong, isolated, continuous reflection arose from an impedance contrast at around this depth throughout the domal core [*Canales et al.*, 2004]. Since velocities of 7.6 km/s and higher would indicate little-altered, olivine-rich rock typical of mantle peridotite [e.g., *Minshull et al.*, 1998], *Collins et al.* [2003] concluded that Moho could be extremely shallow (<1 km) locally within the dome. Third, gravity anomalies indicated that the core of Atlantis Massif has a density that is, on average, 200–400 kg/m^3 higher than the adjacent tectonic blocks [*Blackman et al.*, 1998; *Nooner et al.*, 2003]. Juxtaposition of average crust (2850 kg/m^3) against a mix of altered and fresh peridotite (~3300 kg/m^3) with lesser gabbro could produce this relative density signature. The processing of the regional gravity and seismic data prior to 2004 used standard marine techniques. For gravity, this included the assumption that the density contrast at the seafloor was constant throughout the region [*Blackman et al.*, 1998, 2002]. For the seismic refraction analysis, a presumption of dominant vertical gradients, as opposed to horizontal velocity contrasts, underlay the modeling approach [*Collins et al.*, 2003]. For the MCS processing, a strong mute [*Canales et al.*, 2004] eliminated deeper, more variable reflectivity, which was later shown to occur by *Singh et al.* [2004].

[16] With the geological information available from Site U1309, subsequent geophysical analyses considered additional complexity. This analysis resulted in a model of the Central Dome consistent with all available constraints, including borehole lithology, gravity, and seismic velocity. The postdrilling gravity modeling takes into account the 3-D structure of the hanging wall and domal core at Atlantis Massif (Figure 1c) [*Blackman et al.*, 2008]. The positive 30–40 mGal residual gravity anomaly can be explained if the

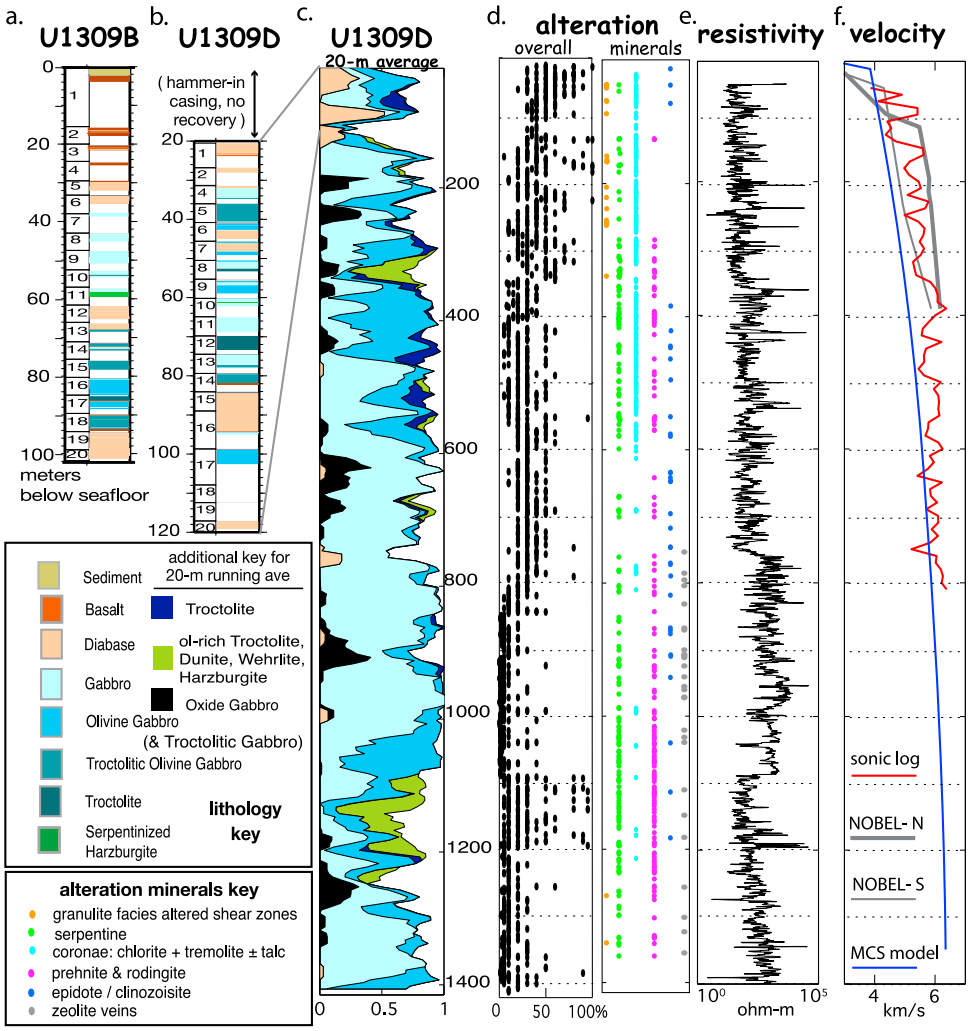

Figure 4. Downhole results at IODP Site U1309. (a) Hole U1309B lithology. (b) Hole U1309D lithology in uppermost section. (c) Hole U1309D lithology with 20 m running average over individual igneous units; white shows fraction of corresponding section that was not recovered. (d) Overall alteration and corona occurrence, from shipboard visual core description, and presence of selected alteration minerals, from thin section log (amount of minerals not shown). (e) Dual laterolog recording of deep resistivity of wallrock in Hole U1309D. (f) Seismic compressional wave velocity. Logged value in Hole U1309D shown by red curve. Profiles extracted from nearby refraction velocity models are also shown (NOBEL, *Collins et al.* [2009]; MCS portion of Line 10, *Blackman et al.* [2009]).

core is gabbroic with density of 2900 kg/m^3, the adjacent basaltic block is significantly fractured with average density 2600 kg/m^3, and the portion of the lithosphere deeper than 1.5 km mbsf that has density lower than mantle rock (either dominantly gabbroic, peridotite that is significantly altered, or a mix thereof) is ~3 km thick within the domal core.

[17] Postdrilling seafloor refraction modeling showed that shallow mantle velocities, although permissive based on the NOBEL data, are not required [*Collins et al.*, 2009] (Figure 3c); velocities in the upper several hundred meters of the new model are typical of mafic rock (≤6.5 km/s). Tomographic inversion of refracted arrivals recorded by the 6 km MCS streamer [*Canales et al.*, 2008] obtained a similar velocity structure to 1.0–1.5 km depth along Lines 10 and 4 (the latter model shown in Figure 3d) where they cross the Central Dome (Figure 2). More detailed analysis of the upper few hundred meters is possible when the MCS refraction data are downward continued, which, in turn, allows greater accuracy of structure determined for the 0.5–1.5 km deep section. Arrival time tomography using downward-continued data for a portion of Line 10 [*Harding et al.*, 2007] confirmed that velocities in the upper 1.5 km of the footwall are 6.5 km/s and lower. The velocity-depth curve for the revised NOBEL model [*Collins et al.*, 2009] brackets the sonic log data for Hole U1309D. A recent MCS tomographic result for Line 10 [*Blackman et al.*, 2009] (Figure 4), 1.8 km to the north of the hole, is similar although velocities are somewhat lower in the interval between 150 and 550 mbsf. Analysis of a 40 km long air gun refraction profile across the Central Dome (approximately along MCS Line 10, Figure 2) subsequently provided coarser constraints on velocities to depths as great as 7 km. Traveltime tomography [*Blackman*

and Collins, 2010] indicated that significant volumes of rock with mantle-like velocity (>7.5 km/s) occur only below ~5 km subseafloor depth within the dome (grading downward within the coverage to 7.8 km/s), and are more than 6 km deep in the axial valley.

[18] We cannot yet confirm the source(s) of the impedance contrast that gives rise to the strong reflection imaged throughout much of the dome (the 'D reflector') [*Canales et al.*, 2004]. Reflectivity modeling based on borehole velocity and density logs [*Collins et al.*, 2009] does produce an arrival from an impedance contrast near an alteration boundary observed in the recovered core from 380 m subseafloor depth in Hole U1309D (Figure 4d). However, the amplitude of this predicted reflection is modest. A more likely candidate for the D reflector may be the base of a thin (~100 m), low velocity layer (~3–3.5 km/s) immediately below the seafloor. *Collins et al.* [2009] showed that such a layer overlies ~5.5 km/s material (Figure 3). This interpretation is similar to one put forward for OCCs in the Philippine Sea [*Ohara et al.*, 2007]. However, complexity due to seafloor scattering in the published reflection image near Site U1309 [*Collins et al.*, 2009], and the offset between Hole U1309D and the closest MCS line (Line 4, ~400 m away) preclude our ability to make a detailed correlation between local rock properties and any given reflector.

[19] Prior to Expedition 304/305, geophysical and geological studies supported the hypothesis that a significant fraction of the subseafloor at Atlantis Massif was ultramafic. In retrospect, the discovery that virtually everything recovered by drilling was mafic suggests that a more comprehensive exploration of alternative structural/lithologic distributions may have resulted in a more complex suite of hypotheses to be tested and could have had an impact on the design of the experiment (drill site selection, borehole experiments, or additional mapping). The surprise and disappointment when mantle was not encountered during Expedition 305 was strongest among researchers who are less acutely aware of the inherent nonuniqueness in most geophysical analyses. However, the geophysical community can also benefit from the experience, if the tendency to rush exciting initial findings to press in a form that does not clearly portray the realm of uncertainties and unknowns can be tempered. This means detailing limits due to both the data and coverage themselves and any assumptions that underlie the processing steps. Whereas the original proposal PIs emphasized OCC structure and evolution in their drilling request and this remained the stated main emphasis for drilling (Table 1) [*Blackman et al.*, 2004], the broader community's interest was probably more strongly captured by the prospect of sampling fresh mantle. Future endeavors where the latter is the target will probably benefit from detailed geophysical analysis and critical review, in light of a range of possible models and hypothesis tests, before finalizing the project plan. However, since the purpose of drilling is to obtain information unattainable in any other way, postdrilling reevaluation of regional data will almost always occur, bringing additional insights on the core and logging discoveries.

5. Summary of Drilling Results

[20] The core and borehole data obtained at Site U1309 contain a wealth of information on the accretion and initial evolution of oceanic lithosphere. Analyses are ongoing and expected to continue for many years. In this section, we provide a summary of postdrilling results to date since the individual studies have been published outside the traditional geophysical literature and each focused on only an aspect of the recovered section. While more detail is available in the original papers, this summary provides a basis for considering the implications discussed in subsequent Sections. We focus on how results thus far inform two aspects of Atlantis Massif's development– magmatic accretion and deformation within ~15 km of the axis of spreading. Some of these results may point to processes specific to periods when OCCs develop, several are likely applicable to slow spread oceanic lithosphere in general.

5.1. New Information on Magmatic Accretion

[21] The uppermost rock types recovered at Site U1309 include diabase and/or basalt that make up 35–40% of recovered core above 120 mbsf (Figures 4a–4b), and that are the sole type recovered from the top ~30 m. These intrusive rocks are little deformed but strongly amphibolitized. They show clear chilled margins against cataclastic gabbro and amphibole-rich fault breccias dominated by metabasaltic clasts, as well as against undeformed diabase. Correlation between Holes U1309B and D suggests that they form sill-like bodies 5–10 m thick dipping at about 30° (Section 5c), an inference supported by preferred alignment of phenocrysts dipping 10°–40° in diabase at 85–100 mbsf. A few steep contacts were recovered from Hole U1309B. *McCaig et al.* [2010] suggested that the latter intrusions occurred subparallel to a steeply dipping fault zone (that later rotated, Section 5b). Other intervals of diabase were sampled throughout the sequence but, below 120 mbsf, they are sparse and their (recovered) thickness rarely exceeds one meter (Figures 4a–4c) [*Blackman et al.*, 2006]. The composition of all diabase recovered falls within the range of basalt compositions for the MAR 30°N axial region [*Godard et al.*, 2009].

[22] The dominantly gabbroic sequence underlying the upper diabase units comprises hundreds of individual lithologic units ranging in composition from gabbro, to oxide, olivine and troctolitic gabbro, troctolite, and olivine-rich troctolite. Each igneous unit was identified during shipboard characterization on the basis of modal composition (Figure 5a) and/or grain size changes downcore. Contacts between units were recovered in many instances (Figures 5c–5d), allowing recognition of relative age. Based on these contact relations, the scale of intrusion varies from centimeters to tens of meters, with the latter thickness being most common [*John et al.*, 2009]. In general, relatively evolved rock types intrude more primitive rock types although the inverse sense of intrusion is also observed locally [*Blackman et al.*, 2006; *John et al.*, 2009].

[23] Leucocratic intrusions (cm-scale thickness) cut the sequence and, together with oxide gabbro intervals, host zircon grains that have been used to obtain crystallization ages of the recovered crustal section. *Grimes et al.* [2008] used an ion microprobe (SIMS) method and $^{206}Pb/^{238}U$ ratios to determine a weighted mean age for the recovered sequence of 1.20 ± 0.03 Ma [*Grimes et al.*, 2008], from which they propose that accretion occurred over a minimum of 100–200 kyr.

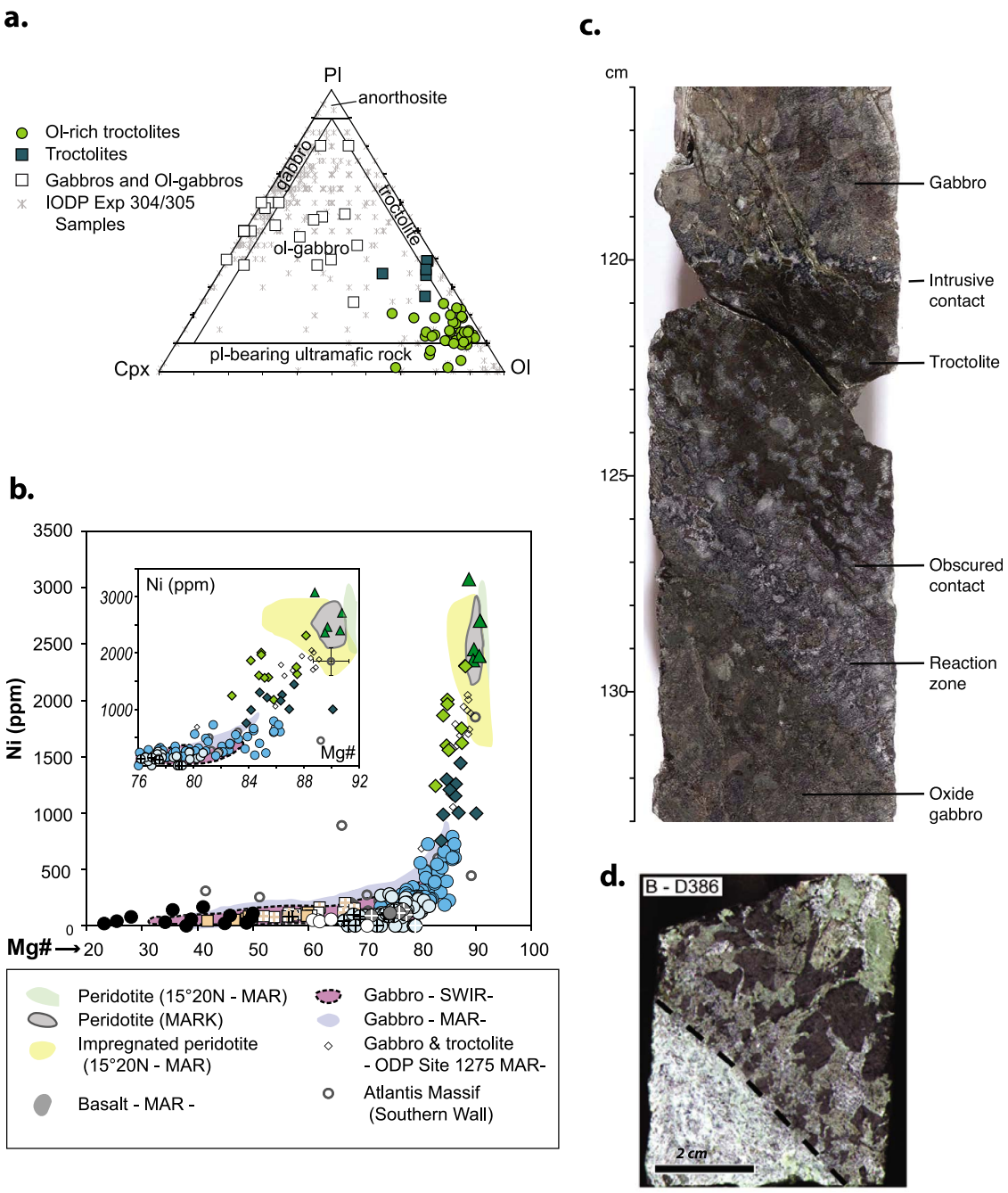

Figure 5. Petrology, geochemistry, and photographs of Site U1309 core samples. (a) Compositions for representative suite of samples from the site are shown by small gray symbols. Other symbols indicate samples from within the intervals that are dominantly olivine-rich troctolite that were studied in detail by *Drouin et al.* [2009]. (b) Bulk rock chemistry for Site U1309 (symbol color key same as Figure 4) and comparison with other areas (shaded fields). [from *Godard et al.*, 2009]. Note how troctolites and olivine-rich troctolites fill in previously sparsely populated Ni-Mg# space. (c) Photo of Core 304-U1309D-69R-1 shows intrusive contact between gabbro and troctolite and lower contact that is a reaction zone between the troctolite and a later oxide gabbro injection. (d) Oxide gabbro dike intrudes gabbro (upper unit) with a sharp lower contact with gabbro [from *Grimes et al.*, 2008].

[24] Modal mineralogy and bulk rock geochemistry (e.g., Figures 5a and 5b) of the gabbroic sequence are typical of a cumulate series crystallizing from a mid-ocean ridge basalt (MORB) source. Observed covariations in plagioclase and clinopyroxene composition between olivine gabbro and gabbro are also typical. However, *Godard et al.* [2009] determined that the bulk composition of Hole U1309D does not represent the complement to basalts recently erupted at the nearby

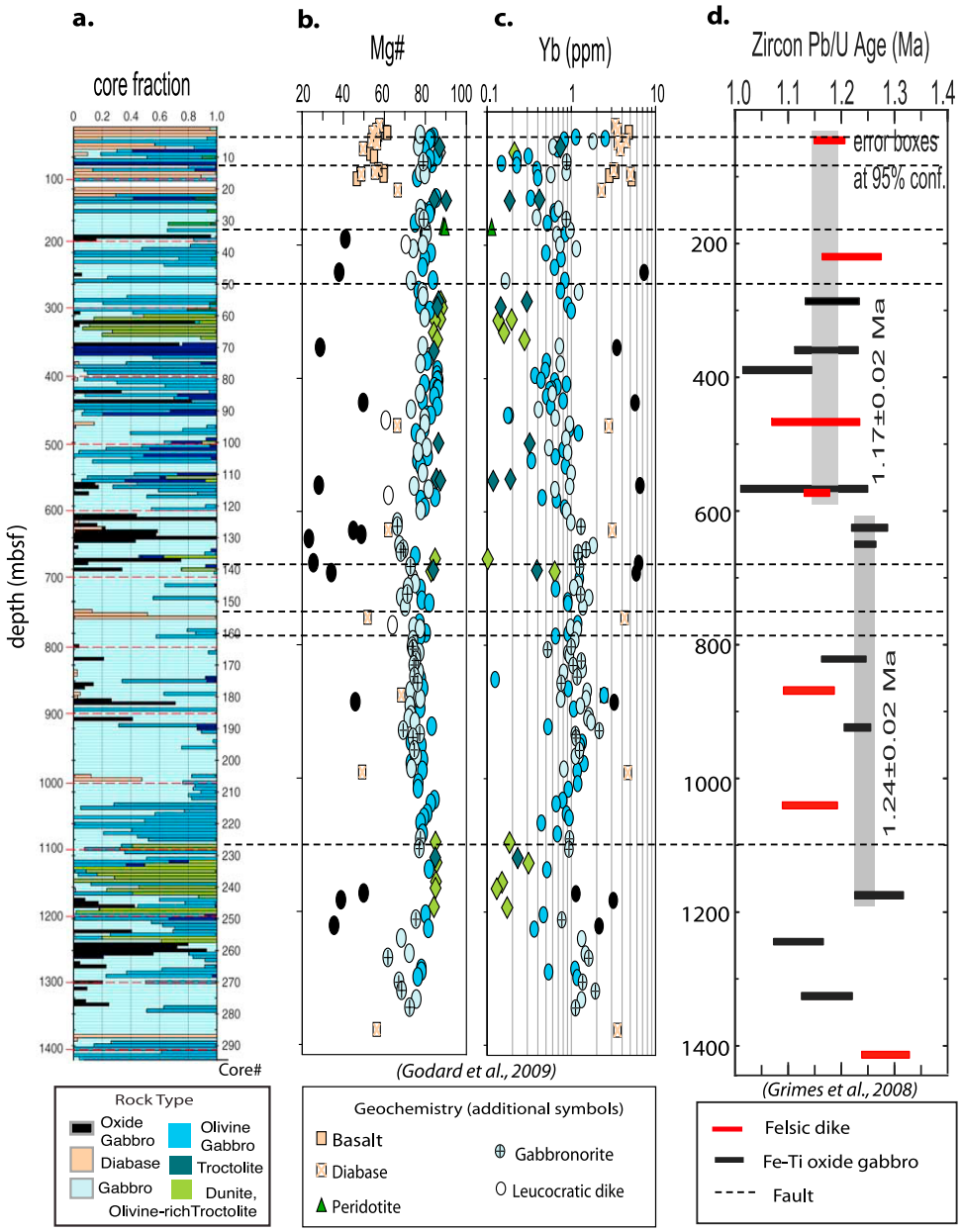

Figure 6. Downhole igneous variation in Hole U1309D. (a) Proportion of rock type recovered in each core section (core number on the right). (b) Bulk rock magnesium number MgO/(MgO + FeO). (c) Bulk rock trace element measurements for Ytterbium. (d) Age dates obtained for core samples. Horizontal dashed lines indicate fault zones inferred from cataclastic deformation or fault gouge in core and (below 35 mbsf) coinciding wall rock structure observed in images (resistivity) or porosity.

spreading axis. On the basis of higher than expected trace element contents, these authors concluded that a significant amount of evolved melt was trapped and crystallized within the sequence. Plagioclase + liquid thermometry yielded a crystallization temperature of 1230 ± 25°C for the troctolite and gabbro [*Drouin et al.*, 2009]. Low-pressure crystallization depths (≲200 MPa, ~6 km) were inferred based on the modal relationships and chemistry of cumulus and intercumulus phases [*Suhr et al.*, 2008; *Godard et al.*, 2009], and have been supported by a combination of rock age dates and assumptions about fault geometry and isotherm depth [*Grimes et al.*, 2011] that put zircon crystallization depths at 5–7 km. *Godard et al.* [2009] noted the complexity of modal composition for the many thin igneous units, and the variability of contact type, ranging from sharp to diffuse, in their preference for a model where the sequence was built by multiple injections of melt. In contrast, *Suhr et al.* [2008] prefer a model where a small number of several hundred meter thick magma bodies each differentiates over a finite period, to provide evolved melts that react with host rock and intrude earlier crystallized intervals.

[25] *Suhr et al.* [2008] interpreted a repeating pattern of olivine gabbro grading upward into a mainly gabbro to

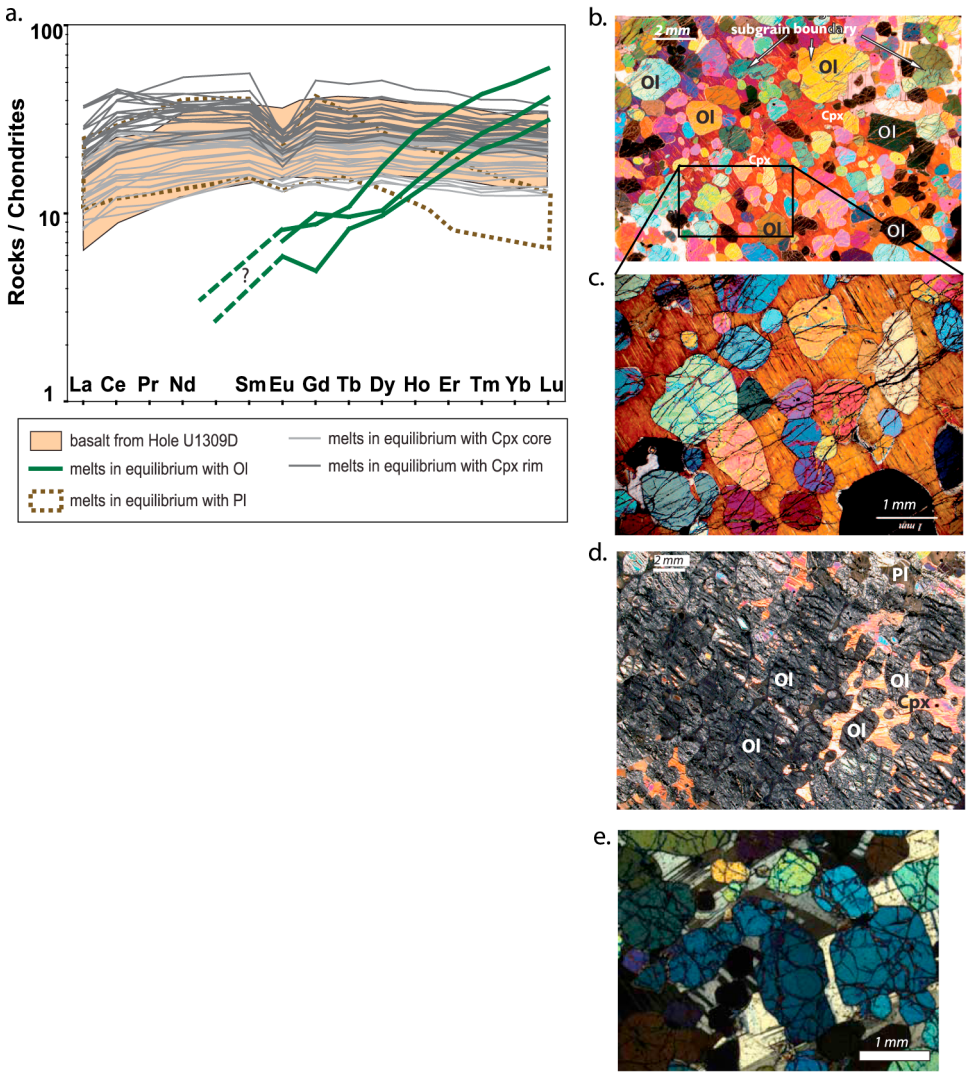

Figure 7. Sample characteristics from olivine-rich troctolite intervals. (a) Computed rare earth element abundances for melts in equilibrium and measured mineral chemistry of samples within these intervals [from *Drouin et al.*, 2009]. Contrast in fields observed and those that would be in equilibrium with olivine (Ol) or plagioclase (Pl) precludes simple cumulate + crystalized melt explanation for the rocks. (b) Round Ol grains within large clinopyroxene (Cpx) in olivine-rich troctolite sample 247R3_16–18. (c) Expanded view highlights chains of corroded olivine within Cpx oikocryst. (d) Serpentinized Ol grains with interstitial Cpx and Pl in sample 64R1_58–60 (Figures 7b–7d from *Drouin et al.* [2010]). (e) Common extinction angle of adjacent Ol grains (blue) and interstitial plagioclase (thin section U1309D-248R2_7).

gabbronorite interval which, in turn, is overlain by a thin oxide gabbro interval (Figure 6a). Mg# (Mg/Mg + Fe) and trace element contents [*Godard et al.*, 2009] support the idea that a staggered sequence of a few magmatic pulses built the recovered section. Decreases in bulk rock Mg# at 640 mbsf and 1235 mbsf coincide with increases in Yb content (Figures 6b–6c), suggesting that these mark possible boundaries of different magmatic units. *Suhr et al.* [2008] prefer to locate the top of the central magmatic body around 800 mbsf, below the fault zone at 750 mbsf, but their analysis did not include the sequence above this fault. The choice of ~640 mbsf as the boundary is similar but not an exact match to a jump in Pb/U zircon ages for Fe-Ti oxide gabbro samples from 1.17 ± 0.02 Ma at 570 mbsf to 1.24 ± 0.02 Ma at 623 mbsf [*Grimes et al.*, 2008] (Figure 6d). Regardless, while repetition of a few hundred m thick intrusions and subsequent self-intrusion during a simple MORB crystallization sequence addresses some of the lithologic variation in the hole, it cannot by itself account for the olivine-rich troctolite intervals.

[26] Olivine-rich troctolite (>70% olivine with low modal plagioclase and clinopyroxene) is present as relatively thin (~1 to 12 m) units within two main intervals (~310–350 mbsf and 1090–1235 mbsf, Figure 6a). Bulk rock geochemical signatures of these troctolites are more primitive than other mafic samples from the ocean crust [*Godard et al.*, 2009]

(Figure 5b). Cumulate textures are observed in the olivine-rich troctolites [*Blackman et al.*, 2006] (Figure 7), but several lines of evidence suggest that these rocks are not simply the first crystallized product of a closed, fractionating magma body. Based on mineral chemistry and textural relations, *Drouin et al.* [2009, 2010] support a model whereby the olivine-rich troctolites formed through open system reaction between initial olivine-bearing rocks and later MORB melts. Trace element patterns for melts in equilibrium with the measured in situ plagioclase, clinopyroxene and olivine compositions (Figure 7a) illustrate that the olivine is in complete disequilibrium with MORB melts that crystallized the plagioclase and clinopyroxene [*Drouin et al.*, 2009]. Whereas modest intracrystalline deformation of olivine grains is observed, surrounding oikocrystic clinopyroxene and plagioclase crystals are undeformed (Figures 7b–7c), indicating that crystallization of the impregnating melt occurred either rapidly or under static conditions. The chemistry of the core of clinopyroxene grains differs from their rim in the olivine-rich troctolite units [*Suhr et al.*, 2008; *Drouin et al.*, 2007, 2009]. Ti is enriched and Al and Cr are depleted toward the rim, whereas plagioclase and olivine grains are unzoned. Using geochemical constraints, *Suhr et al.* [2008] estimated melt:rock ratios around 3:1, with the original host rock being mantle peridotite. *Drouin et al.* [2009] also concluded that high melt:rock ratios characterized the olivine-rich troctolite intervals.

[27] A variety of observations, therefore, demonstrate that the olivine-rich troctolites were produced by infiltration and assimilation of olivine-rich rock by a MORB melt. These are consistent with, but do not prove that the preexisting olivine grains were derived from mantle peridotite. *Drouin et al.* [2010] interpreted the observed relatively stronger concentrations of olivine [001] preferred orientation in some of these rocks to result from dunitization and disaggregation of mantle peridotite which, if not heavily fluxed with melt, would be expected to display flow-induced [100] preferred alignment in this setting. Disruption of preexisting high-temperature crystallographic preferred orientations during melt influx is also suggested by the common occurrence of adjacent grains with neighbor crystallographic orientations. *Suhr et al.* [2008] also noted microstructural evidence in their interpretation of the olivine-rich troctolites as having mantle peridotite origin. They based their conclusion on the fine (0.5 mm) size, and common extinction of adjacent olivine grains (Figure 7e) together with both observed and modeled Cr and Ni geochemistry.

[28] A few thin intervals of mantle peridotite showing lower melt:rock ratios [*von der Handt and Hellebrand*, 2010] were recovered from Site U1309 (<0.5% of the total core; Figure 4), all from above 200 mbsf [*Blackman et al.*, 2006]. Petrologic and geochemical analysis of multiple samples from these intervals [*Tamura et al.*, 2008; *Godard et al.*, 2009] show that three residual harzburgite screens or remnants remain (59, 155, and 174 mbsf) after having been surrounded and impregnated by the gabbroic melt that form the Site U1309 sequence. Three other thin ultramafic intervals are most likely original cumulates (wehrlite, dunite) also penetrated by MORB melts. Together with the results of detailed analyses on the olivine-rich troctolites, the picture that emerges is one where the lithospheric section sampled at the Central Dome of Atlantis Massif was formed piecemeal as a stack of gabbroic bodies intruded into mantle peridotite and earlier solidified gabbro. Associated with this stack are screens of peridotite and larger zones of olivine-rich troctolite that have formed by interaction with gabbroic melt.

5.2. Lithospheric Deformation

[29] In contrast to other sections of ocean lithosphere obtained by drilling at, or in the vicinity, of an OCC (see Section 6), the recovered sequence lacks pervasive deformation, either brittle or plastic [*Blackman et al.*, 2006]. The zones where deformation intensity is 2 or higher (on a scale from 0 to 5, undeformed to ultramylonite/cataclasite) are narrow (cm-to-m scale, Figures 8 and 9) and sparse throughout the core. High strain processes associated with grain size reduction were apparently confined to narrow intervals. We cannot rule out the occurrence of submeter-scale, high-strain intervals that were not recovered in core (white portion of lithology columns in Figure 4), such as intervals 4–16 mbsf in Hole U1309B, 0–20 m and 103–117 mbsf in Hole U1309D. Apart from these intervals, there is no evidence for high strain zones that are several meters thick. Cataclastic structures are more common in the upper part of the core (<750 mbsf) than in the lower part, and a number of thin cataclastic and breccias zones are cut by diabase intrusions in the upper 80 m of the core [*Blackman et al.*, 2006]. Most of the crystal plastic deformation is recorded in the upper 310 m of the section, but the interval 640–700 mbsf and another centered on 1300 mbsf also show plastic deformational structures (Figure 8a). Fault gouge recovered from 750 mbsf has significantly higher intensity cataclastic deformation than any other interval (Figure 8b).

[30] At Site U1309, fragments of talc-tremolite schist sampled only in the uppermost 25 m [*Blackman et al.*, 2006] document intense deformation, with syntectonic growth of phyllosilicates associated with metasomatism and fluid flow. If these represent, as we suggest, an in situ talc-rich deformed zone it would have to be very narrow (≤25 mbsf) based on drilling, coring, and recovery from all the holes at the Site (Figure 2). Brecciation of fine-grained metadiabase at greenschist facies conditions occurred in several intervals within the upper 130 m, but not greater depths. *McCaig et al.* [2010] infer that these basaltic melts were intruded in close proximity to, if not within, a region of faulting. They interpret high $^{87}Sr/^{86}Sr$ and low $\delta^{18}O$ in samples from the upper ~100 m at Site U1309 to indicate high fluid flux within a detachment zone whose activity was coeval with magmatism that produced diabase. This resulted in only highly localized deformation, such as brecciation and the formation of talc-tremolite-chlorite schist. In a later Section (7), we discuss differences between the deformation observed in the upper ~100 m of the Central Dome and that determined to define a detachment shear zone atop the Southern Ridge [*Karson et al.*, 2006].

[31] Of the several narrow fault zones identified in core from Hole U1309D (dashed lines in Figures 6 and 8), the most significant fault is located ~742–761 mbsf [*Michibayashi et al.*, 2008; *John et al.*, 2009], where a continuous 80 cm sample of gouge was obtained, although recovery was generally poor in the interval. Borehole logs (neutron porosity, density, resistivity) suggest that the fault zone could be up

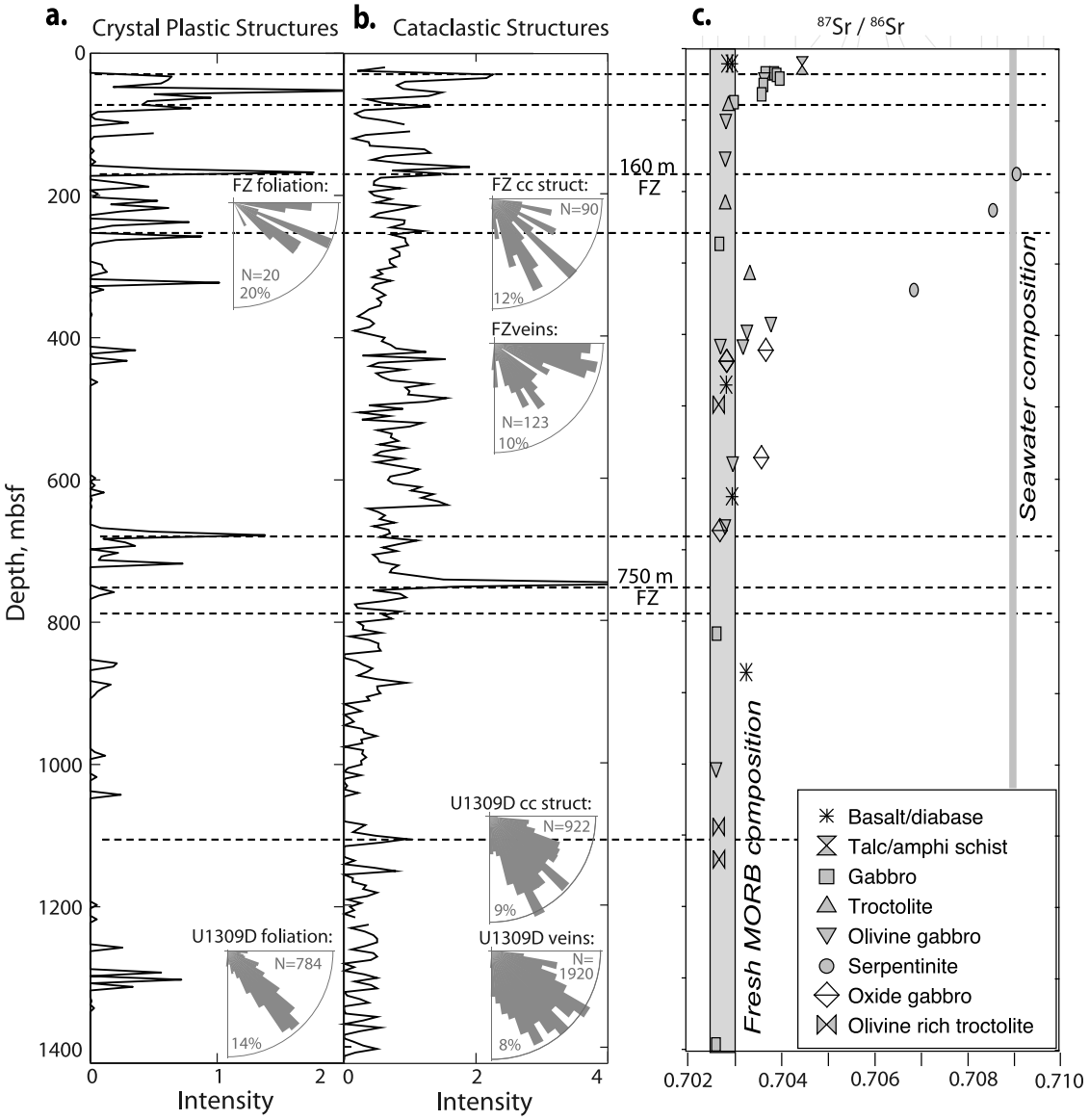

Figure 8. Downhole deformation in core from Hole U1309D [*Hirose and Hayman*, 2008] and evidence of extent of seawater penetration into the formation. (a) Intensity of crystal plastic deformation along core sections on scale of 0–5 (low-high). (b) Intensity of cataclastic deformation along core sections on scale 0–5. Rose diagrams in Figures 8a and 8b show orientation with respect to downhole direction, no correction for paleomagnetically deduced footwall rotation indicated. Upper diagrams refer only to structures measured within the fault zone ~160 mbsf; lower diagrams are for entire hole. (c) Strontium isotope ratios measured on selected core samples with comparison to values for fresh MORB and seawater [*McCaig et al.*, 2010]. Dashed lines indicate fault zones identified on the basis of core and borehole logging information.

to 5 m thick. Permeability of the (ultra) cataclasite is 1–3 orders of magnitude greater than that of adjacent rock types, although not unusual, at 10^{-17}–10^{-19} m^2, for intrusive mafic rock [*Michibayashi et al.*, 2008]. The presence of amphibole together with a local drop in borehole resistivity (Figure 4e) indicates hydration of the zone. *Michibayashi et al.* [2008] determined that seams of aluminous actinolite and plagioclase indicate brittle failure at high temperature (>600°C). The relatively modest permeability is explained by subsequent sealing by hydrous minerals that prevented further circulation and allowed preservation of water in the crust.

[32] Paleomagnetic data provide constraints on tectonic rotation experienced by the footwall rocks. Remanent inclinations of core samples are approximately 10° shallower than expected for reversely magnetized rock at the site, suggesting significant tectonic rotation since acquisition of magnetic remanence. IODP cores in igneous rock are not azimuthally oriented so magnetic declinations cannot ordinarily be determined. However, it has been possible to independently reorient a number of core pieces by matching oriented borehole features imaged with the Formation MicroScanner to features observed in core pieces. *Morris et al.*

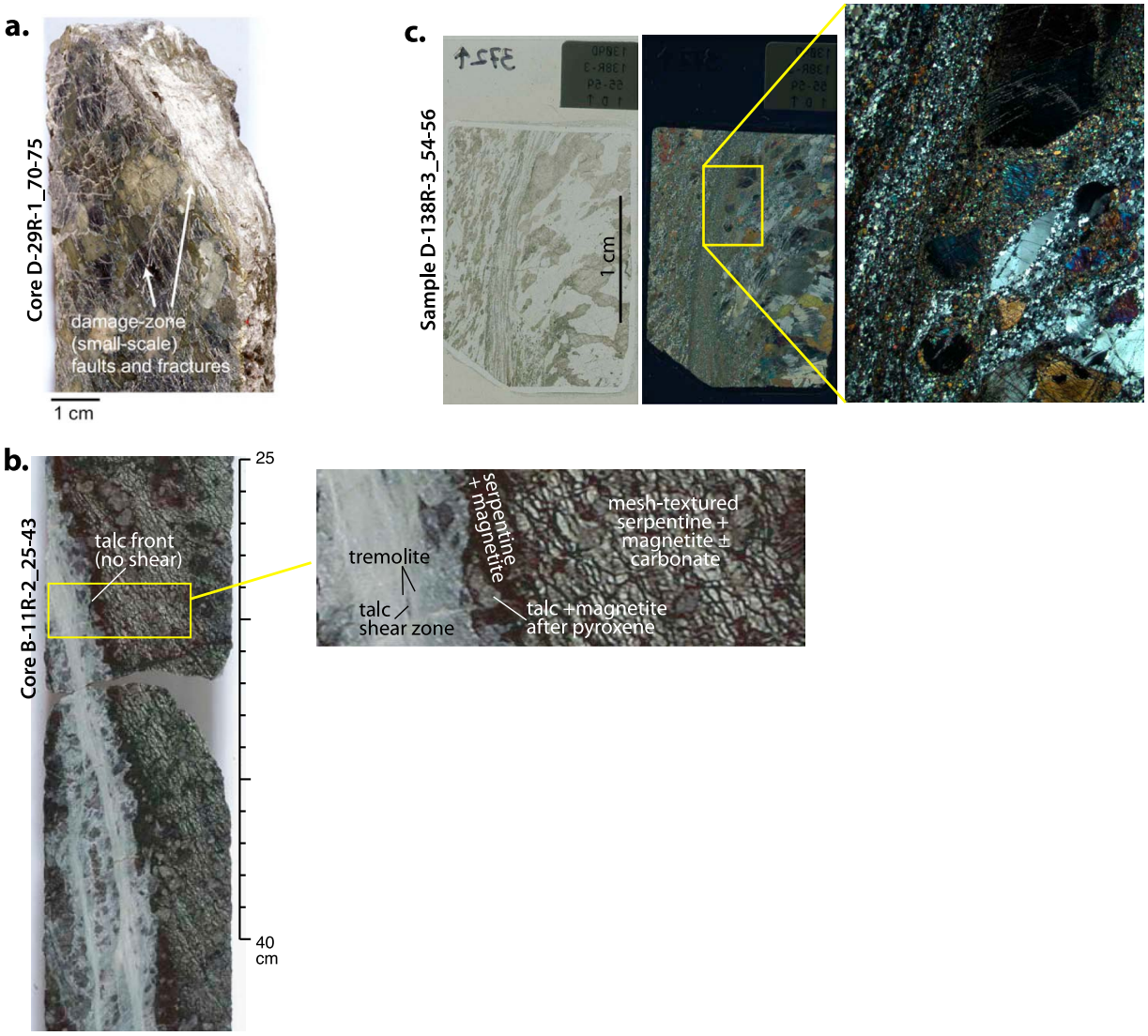

Figure 9. Deformation at Site U1309. (a) Talc in shear zone at ~160 mbsf where fault cuts gabbro [from *Hirose and Hayman*, 2008]. (b) Tremolite and talc along shear zone in serpentinized harzburgite. Reverse shear occurred along talc-rich horizons, but the margin of talc alteration against serpentinite + magnetite is unsheared. (c) Crystal plastic deformation with sharp contact at edge of 2 cm wide shear zone: plain light, XPL, thin section [modified from *Blackman et al.*, 2006].

[2009] report results for 34 samples from the upper 400 m of the section. The mean full remanence vector from these oriented samples has a southwesterly declination and indicates a minimum of ~45° counterclockwise rotation about a horizontal axis oriented 011° (ridge axis parallel). Although shipboard measurements imply that most core samples from the upper 180 m have magnetic inclinations close to that expected, the reoriented data from this interval have declinations displaced to the SW, thus rotation is required. Interpretation of inclination data from the 400–1415 mbsf interval, and incorporation of directional constraints from local seafloor corrugations [*Garcés and Gee*, 2007] yield an essentially identical amount of rotation. Using average paleomagnetic inclinations alone, *Zhao and Tominaga* [2009] suggest rotation up to ~50°. These results demonstrate that the footwall experienced significant overall rotation since acquisition of magnetization (i.e., below 550°C), consistent with flexural rotation during exposure of the detachment at the seafloor. The magnitude of rotation recorded by the paleomagnetic results from the Central Dome is comparable to what has been inferred from seafloor morphology modeled as blocks back tilted via slip along a detachment fault [*Smith et al.*, 2008; *Schouten et al.*, 2010].

[33] The large footwall rotation, certainly for the upper 400 mbsf [*Morris et al.*, 2009] and inferred for the full 1.4 km section [*Morris et al.*, 2009; *Zhao and Tominaga*, 2009], combined with the little deformed nature of the Site U1309 drill core suggest that at least this (upper) portion of the footwall behaved as a relatively coherent block during OCC formation. Flexural bending and/or sustained fault slip that enabled the rotation must have resulted in fracturing, folding, or shearing in a region that is either very localized in

the upper 25 m of the core, which was almost unsampled, or outside the drilled zone.

[34] *Grimes et al.* [2008] considered the issue of footwall rotation in their discussion of the ages obtained from oxide gabbro and felsic dikes within the sequence (Figure 6d). They suggested that the lack of systematic younging upward ages indicates that two main periods of multiinjection sill intrusions occurred at different subaxial depths (forming present-day rock intervals above and below ~600 mbsf, respectively). These authors then investigated models of magma emplacement depth and possible active detachment fault geometry to assess what the mean rock age might indicate in terms of asymmetry in lithospheric extension during OCC formation. They conclude that for a minimum of a few hundred kyr period when a detachment fault served as the main plate boundary, movement of the footwall along the western ridge flank accounted for 70–100% of the relative motion across the spreading axis. They inferred that the asymmetry in west versus east flank spreading rates decreased over the past 1 Ma, as slip along the detachment ceased.

5.3. Comparison Between Hole U1309B and Upper Hole U1309D

[35] The recovered rock sequences from Holes U1309B and U1309D do not correlate simply [*Blackman et al.*, 2006] (Figures 4a–4b). The lateral scale of thin, interfingered gabbroic units sampled in each hole therefore must be less than the 20 m offset between holes, or disruption with a significant vertical component separates the two areas. The thin harzburgite unit recovered at 60 mbsf from Hole B is not directly equivalent to the peridotite recovered from 62 mbsf in Hole D, which is wehrlitic [*Blackman et al.*, 2006; *Tamura et al.*, 2008; *Godard et al.*, 2009]. However, phenocryst alignment and downhole patterns of magnetic susceptibility suggest that some of the diabase units trend upward from Hole B and are intersected at depths ~11 m shallower by Hole D to the north [*Blackman et al.*, 2006]. This indicates that diabase units within the domal core can sometimes be laterally continuous over distances greater than the size of the gabbro units forming the upper 100 m at Site U1309 and that their current disposition has a component of dip that is ~29° toward the south.

5.4. Conditions During Exhumation of the Domal Core

[36] The signatures of changing pressure/temperature conditions, and the extent of fracturing within the domal core as unroofing and uplift proceeded are recorded as alteration assemblages in the footwall rocks. All rocks in the massif have experienced the complete range of metamorphic temperatures from magmatic to ambient conditions, so the distribution of metamorphic assemblages documented by *Blackman et al.* [2006] reflects a combination of the timing of fluid access and the time spent in different temperature intervals. Note that the discussion of facies in this paper follows common usage in studies of ocean floor metamorphism (i.e., hornblende-bearing metamorphic rocks are typically referred to as amphibolite, while actinolite-bearing rocks are referred to as greenschist). This usage, in part, reflects the difficulty of obtaining accurate temperature and pressure estimates in low-pressure rocks where water activity can vary widely in both time and space.

[37] Granulite and upper amphibolite facies ductile deformation was extremely limited, and more or less confined to the upper part of the sequence (Figures 4d and 10c). These shear zones have not been thoroughly studied, but likely formed at temperatures in excess of 750°C.

[38] Static hydration began in the amphibolite facies, continued in the greenschist facies, and was pervasive in the upper part of the sequence, above about 300 mbsf (present-day depth), where reactions such as tremolite-chlorite corona formation between olivine and plagioclase generally continued until one of the reactant phases was consumed. The intensity of both mineralogical and isotopic alteration decreases significantly below this depth, and completely fresh gabbros are common beneath the fault zone at 750 mbsf (Figures 4 and 8). At these depths, fluid access was restricted to faults [e.g., *Hirose and Hayman*, 2008; *Michibayashi et al.*, 2008], veins, and igneous contacts (e.g., resulting in serpentinization of parts of olivine-rich troctolite layers). The concentration of alteration in the vicinity of late felsic intrusions may also reflect exsolution of magmatic fluids.

[39] Additional data is required to establish the full distribution of amphibolite vs greenschist facies hydration within the sequence [e.g., *Nozaka and Fryer*, 2011], but most samples studied to date contain amphibole showing a wide range of composition reflecting a broad range of temperature conditions [e.g., *Blackman et al.*, 2006; *Michibayashi et al.*, 2008]. Alteration halos (Figures 10a and 10b) around several veins/igneous contacts from depths 433–1376 mbsf have been studied in detail by *Nozaka and Fryer* [2011]. The halos are zoned with tremolite pseudomorphs after olivine present throughout the inner zone, some overgrown by green hornblende, and thick chlorite along adjacent plagioclase boundaries. Talc replacement of olivine is typical within the second zone. The third zone, most distant from the vein/contact, has tremolite and chlorite along boundaries of adjacent olivine-plagioclase grains and relict olivine is observed (Figure 10b). *Nozaka and Fryer* [2011] propose that the tremolite-chlorite coronas formed at temperatures between 450 and 650°C, somewhat higher than the range implied by *Blackman et al.* [2006]. Overprinting hornblende is interpreted to reflect a period of prograde metamorphism with temperatures rising to around 750°C. Cataclasis in the fault zone at 750 mbsf also appears to have occurred in the amphibolite facies, with *Michibayashi et al.* [2008] estimating an amphibole-plagioclase temperature of 640°C. Microrodingite assemblages (Figure 10d) that postdate corona formation occurred below 350°C [*Frost et al.*, 2008], while initial serpentization involving antigorite may have occurred above 300°C, continuing to lower temperatures with growth of lizardite and magnetite replacing early Fe-bearing brucite (Figure 10e) [*Beard et al.*, 2009]. Tremolite-talc veins in ultramafic horizons in the upper part of the core (Figure 9b) show similar assemblages to detachment fault rocks [*Escartín et al.*, 2003; *Boschi et al.*, 2006]. Talc at the edge of the vein in Figure 9b contains magnetite inclusions, suggesting it replaced serpentine. This may also have been a prograde event, although further work is required to establish this.

[40] Hydration at temperatures below 250–300°C was restricted to late clay filled fractures, that are most abundant below about 400 mbsf [*Nozaka et al.*, 2008], and to zeolites which are fairly abundant below 700 mbsf (Figure 4), but have not been proved by XRD at shallower levels. Saponitic

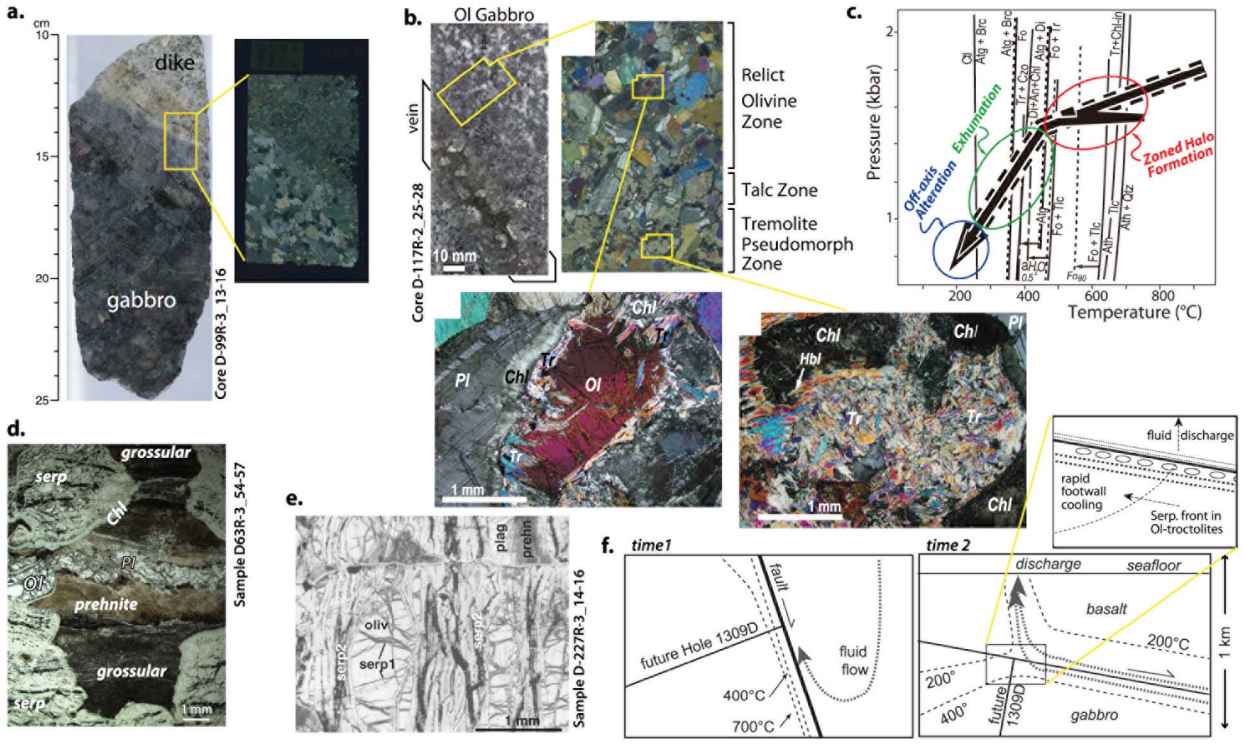

Figure 10. Alteration at Site U1309. (a) Alteration front where leucocratic dike intruded gabbro [modified from *Blackman et al.*, 2006]. (b) Zoned halo surrounding leucocratic vein; tremolite pseudomorph zone is closest to vein. (c) P-T history of core >350 mbsf (Figures 10b and 10c modified from *Nozaka and Fryer* [2011]). (d) Olivine-rich troctolite thin section shows prehnite-grossular-chlorite assemblage associated with serpentinization [after *Frost et al.*, 2008]. (e) Two stages of veins in 50–70% serpentinized sample [from *Beard et al.*, 2009]. (f) Thermal history of the detachment footwall interpreted in terms of cooling by hydrothermal fluid flow up the fault and episode(s) of fluid discharge to seafloor that impact gradient (based on *McCaig et al.* [2010], where fault and fluid flow patterns are inferred on basis of seismicity and venting, respectively, at TAG hydrothermal field).

clay and zeolites probably reflect ambient conditions [*Nozaka et al.*, 2008], where temperatures of at least 120°C are present at 1400 mbsf [*Blackman et al.*, 2006]. The predominance of alteration at temperatures >250°C is confirmed by the lack of whole rock $\delta^{18}O$ values greater than +5.5 ‰ [*McCaig et al.*, 2010]. Sr isotopic alteration is most intense in gabbroic rocks, tremolite schists and serpentinites in the upper 100 m of the core [*McCaig et al.*, 2010] (Figure 8c), suggesting relatively high fluxes of seawater-derived fluids in this zone.

[41] Pervasive alteration in the upper part of the sequence occurred mainly under decreasing temperature conditions in the amphibolite and upper greenschist facies [*Blackman et al.*, 2006], with alteration penetrating further from the detachment fault with time. This may have been mainly lateral penetration away from a steep detachment fault at the time of alteration (Figure 10f). *Nozaka and Fryer* [2011] suggest that green hornblende overprinting tremolite within the zoned halos below 350 mbsf indicates prograde metamorphism after initial hydration. Talc and perhaps tremolite apparently replacing serpentine (Figure 9b) may also reflect a prograde event in the upper part of the sequence. The fact that late diabase and basalt intrusions chill against amphibole-rich breccias of metagabbro and metadiabase shows that magmatism and hydrothermal activity were occurring at nearly the same time. Prograde events may reflect either the direct effects of intrusions or flow of hot fluids related to intrusions at depth [*Nozaka and Fryer*, 2011]. *McCaig et al.* [2010] suggest that flow of hydrothermal fluids through the fault zone buffered temperatures to around 400°C, promoting rapid initial cooling of the footwall from magmatic temperatures but slower cooling through the amphibolite and upper greenschist interval (Figure 10f). Rapid final exhumation of the massif onto the seafloor quickly established an ambient thermal gradient of around 100°C/km, leading to the cessation of metamorphism in the upper part of the sequence and growth of clays and zeolites at deeper levels.

[42] Radial microfractures localized around altered olivine grains indicate that volume increase associated with serpentinization enhances general seawater access into gabbroic rocks [*Blackman et al.*, 2006; *Nozaka et al.*, 2008]. Similar volume increase appears to have promoted both the tremolite-chlorite corona textures in troctolite [*Blackman et al.*, 2006], and perhaps the serpentine-microrodingite "ladder veins" described by *Frost et al.* [2008]. Reaction-enhanced permeability caused by volume increase reactions may have promoted pervasive access of fluid to relatively unfractured

rocks, but the locally enhanced hydration along narrow shear zones indicates that significant fluid flow is confined to these intervals [*Hirose and Hayman*, 2008]. The juxtaposition of highly altered zones against intervals showing little or no alteration is important. Specific examples include (Figure 4): the moderately fresh olivine gabbro interval at 380–400 mbsf, the sharp contrast in alteration of the 1090–1235 mbsf olivine-rich interval and gabbro on either side, and the presence of some very fresh gabbro and olivine-rich troctolite samples within this olivine-rich troctolite zone. Sharp contrasts in borehole resistivity also suggest such juxtaposition of highly altered rock and intervals with little metamorphism (Figure 4e, depths of 380, 750, and 1080 mbsf, where jumps of an order of magnitude (ohm-m) occur across 5–15 m length intervals). *Hirose and Hayman* [2008] propose that this pattern of alteration requires that fluid flow is either restricted to zones that are very narrow (cms to ~1 m), and/or that a self-sealing mechanism accompanies fluid transfer in the fractured zones.

6. Implications of Drilling Results

[43] Following a synopsis of the inferences about the structure, lithology, and evolution of Atlantis Massif drawn from our postdrilling analyses, we discuss the extent to which drilling results addressed the initially targeted hypothesis tests, as well as some additional implications for the site and comparison with other deep drilling results at OCCs.

[44] 1. The main geochemical characteristics of Site U1309 gabbroic rocks are consistent with formation as a cumulate sequence built from a series of parental MORB melt injections [*Godard et al.*, 2009]. Self-intrusion of cooling, partially crystallized magma likely occurred, and infiltration of evolved melt from a given intrusion into preexisting mafic cumulate rock certainly occurred.

[45] 2. The age of zircon-bearing core samples [*Grimes et al.*, 2008] is consistent with formation in the axial zone and a period of asymmetric spreading, with the footwall to a detachment fault moving at or near the full spreading rate for the segment.

[46] 3. The few thin peridotite intervals transected at Site U1309 are residual, but petrographic and geochemical evidence indicate later-formed or injected melts fluxed the residuum [*Godard et al.*, 2009] or infiltrated it as dikelets [*Tamura et al.*, 2008].

[47] 4. Olivine-rich troctolites are the product of intense melt-rock interactions between an olivine-rich protolith (either ultramafic cumulate or mantle peridotite) and basaltic melt [*Suhr et al.*, 2008; *Drouin et al.*, 2009, 2010]. They cannot simply be the primitive, first crystallized cumulate within cooling magma. Such melt-rock interaction processes are expected to play a significant role in crustal accretion at slow-spreading ridges, hence to contribute through melt-rock interactions to MORB chemistry [*Lissenberg and Dick*, 2008; *Drouin et al.*, 2010].

[48] 5. A distinct decrease in alteration with depth indicates pervasive seawater infiltration only in the upper ~380 m. The consistent >40%, low temperature alteration in the upper section gives way to moderate levels of alteration in the interval 400~750 mbsf [*Blackman et al.*, 2006]. Below 800 m, alteration is quite localized and many intervals are very fresh. This indicates that fracturing and seawater infiltration associated with core complex formation does not occur equally throughout the whole young lithosphere. Rather, the highest water-rock ratios are recorded in the now-exposed detachment zone [*McCaig et al.*, 2010] and alteration at depth is confined to local zones [*Nozaka and Fryer*, 2011].

[49] 6. Paleomagnetic data indicate at least 45° counterclockwise rotation of the footwall with tilt occurring about a MAR-parallel horizontal axis [*Morris et al.*, 2009].

[50] Table 2 charts the sequence of processes and conditions that the drilled section experienced, as constrained by shipboard and postcruise results. Returning to the objectives laid out for the IODP Expeditions to Atlantis Massif, our results provide a test of many, but not all, of the hypotheses outlined in Table 1.

6.1. Hypotheses 1, 2, and 5

[51] Any high-strain portion of the detachment zone at Site U1309 appears to be less than 25 m thick, as we recovered few strongly deformed fault rocks from the 1415 mbsf interval cored. While only a few fragments of fault rock were actually recovered within a few meters of the seafloor, we cannot rule out the possibility that we simply did not recover a potentially greater amount of likely fragile rock, due to difficult conditions that prevail when starting a deep hole with a drilling vessel. Seismic tomography [*Collins et al.*, 2009; *Blackman et al.*, 2009] (Figure 3) indicates that a low velocity top interval about 100 m thick characterizes at least parts of the Central Dome. The reduced velocity could be explained by alteration and/or brecciation within a broader detachment zone although we cannot rule out increased porosity associated with exposure at the seafloor.

[52] Paleomagnetic data confirm that the footwall to the detachment fault likely rotated >45° [*Morris et al.*, 2009], consistent with a rolling hinge model and flexural rotation [e.g., *Wernicke and Axen*, 1988; *Buck*, 1988]. Fully oriented samples are not available in the upper ~100 m and analysis is still underway for the 400–1400 m interval, although inclinations for the latter are consistent with this interpretation. If the proportion of serpentinized peridodite recovered from Hole U1309D is representative of the bulk composition of Atlantis Massif, expansion of altered peridotite does not contribute significantly to uplift of the Central Dome.

6.2. Hypothesis 3

[53] The lack of extrusive rock or another caprock above the intrusive complex at Site U1309 confirms that at least some unroofing has occurred. While current results do not definitively pin down the depth of emplacement, the rocks clearly were intruded deep enough for slow crystallization. The alteration history [*Nozaka et al.*, 2008; *Nozaka and Fryer*, 2011; *McCaig et al.*, 2010] indicates rapid cooling through the granulite facies, followed by slower cooling through amphibolite and greenschist facies. This was followed by rapid uplift, to conditions where zeolite facies metamorphism prevailed under ambient conditions in the lower part of the Hole U1309D sequence.

6.3. Hypothesis 4

[54] Expeditions 304/305 mark the third time that deep drilling of a corrugated oceanic core complex produced a

Table 2. Sequence of Processes Documented by IODP Drilling Results[a]

Process	Constraint From Drilling Data
	Subaxial Magmatism
2–3 larger intrusions, total >1.4 km thick	different zircon dates (1.17/1.24 Ma) above/below ~600 mbsf; downhole change in Mg# & Yb ~600–650 mbsf; repeating pattern uphole, from less- to more-evolved rock type
Many small (self) injections of melt	hundreds of individual petrologic units; evolved rock type generally intrudes less evolved type
Melt fluxes preexisting olivine-rich rocks	troctolite olivine grains not in equilibrium w/ interstitial plagioclase; all (sparse) peridotites have later melt crystallized within them
Crystallization of main intrusions	1230 °C, <200 MPa
	Alteration and Strain Localization
Minor shearing at higher temperature	brown hornblende, clinopyroxene, orthopyroxene, olivine, plagioclase all stable in thin mylonites; T > 800 °C; rapid cooling through this interval
Static hydration and cataclasis mainly in a progressively cooling regime, some fluctuations	wide range amphibole compositions: green hornblende-actinolite replacing pyroxene; tremolite-chlorite corona replace olivine & plagioclase; Locally, hornblende overprints tremolite in coronas & talc+tremolite replaces serpentine (up-T reactions). T 750–400 °C
Detachment formation	poorly sampled talc-tremolite schist with ultramafic protolith, same properties as seafloor detachments mapped elsewhere. Amphibole-rich breccia/cataclastic zones cut by basalt/diabase intrusions suggest detachment faulting in gabbro and diabase
Uplift, flexure, exposure of detachment fault; rapid cooling to ambient gradient (~100 °C/km)	Corona reactions replaced by serpentine (antigorite, then lizardite + brucite, then lizardite plus magnetite) and microrodingites at 200–350°C. Late clay-filled veins concentrated in lower part of core. Zeolites only found deeper than 700 mbsf. Palaeomagnetic rotations of 45° since cooling below Curie Point
	Continued Exhumation
Weathering, sedimentation of fault at seafloor	talc-tremolite schist fragments, fossiliferous deposits and hyaloclastic debris
Low-T alteration	alteration of halos surrounding leucocratic veins, clay veining; lizardite veins in serpentinized olivine-rich troctolite ~1090 mbsf

[a]See text for details, uncertainties, and references.

significant thickness of gabbro in an area where mantle ultramafic rocks are exposed on the seafloor nearby [*Dick et al.*, 2000; *Kelemen et al.*, 2007]. This led to our revised model of OCC formation [*Ildefonse et al.*, 2007a], which predicts that a local increase in magma supply to a portion of the segment that is normally less magmatically robust is an important factor in long-lived strain localization within the axial zone. A series of melt injections at depth, over a period of at least a few hundred kyr [*Grimes et al.*, 2008], is hypothesized to form a gabbroic body that behaves rather coherently. Strain is focused around the margins of the composite 'batholith' where alteration by fluids locally reacting with surrounding peridotite country rock significantly reduces its strength [*Escartín et al.*, 2001; *Jöns et al.*, 2009; *Nozaka and Fryer*, 2011].

[55] While the drilling results were a basis for the *Ildefonse et al.* [2007a] hypothesis, a number of questions remain. The multikm scale of the domal cores of many OCCs suggests that the size of the gabbroic body is comparable, if the 'ball bearing' analogy is appropriate. Seismic tomography of the upper ~1.5 km [*Canales et al.*, 2008; *Henig et al.*, 2009] confirms that shallow high velocity, such as would typify mafic intrusive rock, is present within the domal core of Atlantis Massif. However, this velocity-depth signature does not extend the full cross-strike length of the OCC. Recent numerical modeling [*Buck et al.*, 2005; *Tucholke et al.*, 2008] may provide a framework for interpreting this variability if the velocity structure documents a level of magmatism accommodating 30–50% of spreading while large offset faulting takes up the rest. Note that samples from the conjugate crust on the outside corner across from Atlantis Massif have not yet been obtained. These will be crucial for understanding how magma may or may not have been partitioned within the axis or with respect to the detachment fault.

6.4. Hypothesis 6

[56] Reanalysis of geophysical data [*Blackman et al.*, 2008; *Canales et al.*, 2008; *Collins et al.*, 2009; *Henig et al.*, 2009] indicates that there is not a shallow (<1 km) regional Moho at Atlantis Massif. Since the seismic boundary was not transected, we cannot address its geologic properties. As noted in Section 4, the lateral heterogeneity that characterizes slow spread crust, particularly at OCC, invalidates some of the simplifying assumptions that often influence initial marine geophysical modeling. More in-depth analysis of the predrilling geophysical data would have clarified the range of viable interpretations. This could have aided decision making, and, assuming the experiment was still high priority, may have suggested alternate/additional strategies for drilling/logging.

6.5. Hypothesis 7

[57] The recovery of 1415 m of gabbro from the Central Dome, where seismic velocities in the upper ~1 km are found to be higher than normal for young Atlantic crust [*Canales et al.*, 2008], and the similarity of the velocity structure determined for the eastern part of the Southern Ridge [*Henig et al.*, 2009], where the largest residual gravity anomaly is found [*Blackman et al.*, 2008], indicates that

fresh peridotite is not the source of the gravity high. Instead it is the fact that intrusive mafic rock, whose inherent porosity is lower than typical upper crustal volcanic rock, is exposed at the seafloor within the Central Dome. Both the porosity contrast and the greater density of gabbro compared to basalt contribute to the relative anomaly between the dome and the adjacent hanging wall blocks.

[58] The inclusion of very thin screens of mantle peridotite within the km-scale gabbroic sequence drilled at IODP Site U1309, in combination with the bulk composition of the Hole not being the more primitive cumulate complement of MORB sampled in the current median valley documents the complexity of slow spread lithosphere formation/evolution. Models where the large majority of basaltic melt that forms during subaxial partial melting rapidly segregates and migrates to an overlying, upper crustal layer must be modified. Some melt appears to react extensively with its matrix minerals and some crystallizes in place. While we cannot rule out incorporation of some of the thin mantle screens as fault slivers, the impregnation and reactions observed within the olivine-rich troctolite intervals indicate that deep lithosphere forming within the axial zone can be infused with injections of melt. Drilling results at Atlantis Massif support models where emplacement of gabbroic plutons within slow spread ocean lithosphere [e.g., *Cannat*, 1993] is accompanied/followed by faulting [*Cannat et al.*, 1997; *Lagabrielle et al.*, 1998], which eventually exposes these rocks at the seafloor. The degree (cumulatively, ~3:1 melt:residual ratio) and scale (intervals occur within zones that extend a few tens of meters) of impregnation observed within the upper 1.4 km at Site U1309 suggest an axial region where intrusions exceeded deformation of mantle lithosphere under amagmatic conditions. This type of constraint has not previously been clear for an OCC, where the genesis of material contained in footwall is key to understanding the interplay between magmatism and tectonism during its evolution.

[59] Despite undergoing major faulting, rotation, and significant uplift, the domal core of Atlantis Massif is not pervasively deformed or altered. The interplay between fluid circulation (alteration) and strain localization acted to protect large portions of the shallow lithosphere. Metasomatism appears to concentrate along the detachment fault zone and the boundaries between gabbroic and peridotite host rocks [*Bach and Klein*, 2009; *Boschi et al.*, 2006; *McCaig et al.*, 2007] rather than permeating throughout the footwall to the detachment.

[60] The first-order similarity of OCCs that have been drilled to date by ODP and IODP is the occurrence of gabbro plutons in the domal core [*Ildefonse et al.*, 2007a, 2007b]. The most spectacular difference between the Atlantis Bank OCC in the Indian Ocean [*Dick et al.*, 2000], and the OCCs in the Atlantic (15°45′N, and Atlantis Massif) documented by shallow coring [*MacLeod et al.*, 2002] and/or deep drilling [*Blackman et al.*, 2006; *Kelemen et al.*, 2007] is the proportion of crystal plastic deformation recorded in the gabbroic sequence; the core from ODP Hole 735B (Atlantis Bank) [*Dick et al.*, 2000] displays a thicker (up to many tens of meters) protomylonitic to mylonitic shear zone at the top of the section, as well as many more shear zones down section. In contrast, deformation in cores from Atlantic OCCs, in particular in samples from directly beneath detachment faults, occurred at much colder conditions [*Escartín et al.*, 2003; *Ildefonse et al.*, 2007a; *Miranda and Dilek*, 2010; *McCaig et al.*, 2010]. The contrasted metamorphic and deformation history can be summarized in a simple typology of OCCs [*Escartín et al.*, 2003; *Miranda and Dilek*, 2010; *McCaig et al.*, 2010], with the Atlantis Bank representing a "hot" end-member for detachment faults with extensive mylonitization at temperatures >800°C [*Dick et al.*, 2000; *Mehl and Hirth*, 2008; *Miranda and John*, 2010], while the Atlantis Massif and 15°45′N represent a "cold" end-member where gabbro was intruded into the roots of a hydrothermal system controlled by the detachment fault. The greater extent of mylonitic deformation in gabbroic rocks on the South Wall of the Atlantis massif [*Schroeder and John*, 2004; *Karson et al.*, 2006] (see also section 7.1) would then be explained by the intrusion of the Central Dome gabbro after and across this ductile shear zone that represents deeper parts of the detachment fault [*McCaig et al.*, 2010]. An alternate to this characterization put forward by *John and Cheadle* [2010] suggests that the presence or absence of zones of high strain mylonite is likely dictated by several factors including position relative to the breakaway (i.e., initial structural depth), magnitude of slip, rheology (whether dominated by mafic or felsic rocks types), and the involvement of water promoting plastic deformation, during fault zone evolution.

7. Drilling Results in the Context of Regional Data

7.1. Comparisons Between Southern Ridge and Central Dome

[61] There are significant differences in seafloor depth, lithology, deformation, and alteration between the Central Dome and the well-mapped face of the central part of the Southern Ridge of Atlantis Massif (Figures 1 and 2) [*Schroeder and John*, 2004; *Boschi et al.*, 2006; *Karson et al.*, 2006]. Whereas serpentinized harzburgite constitutes <1% of the sequence recovered at Site U1309, serpentinized harzburgite composes >50% of the sample suite obtained by submersible/dredging on the south wall [*Blackman et al.*, 2002; *Boschi et al.*, 2006]. *Delacour et al.* [2008] and *McCaig et al.* [2010] evaluated Sr and Nd ratios for Site U1309 and several south wall samples. They note that high fluid flow with associated alteration and strain localization characterize the South Wall samples but is less intense within the Central Dome sequence sampled. Based on widespread talc-amphibole-chlorite assemblages within the detachment shear zone atop the Southern Ridge, *Boschi et al.* [2006] conclude that extensive metasomatism accompanied deformation that varied from crystal plastic to cataclastic in this zone. *Boschi et al.* [2006] emphasize the importance of mafic-ultramafic interactions in such high exchange zones where deformation occurred in the ~100 m thick detachment shear zone capping the South Wall [*Schroeder and John*, 2004; *Karson et al.*, 2006]. If an exposed detachment caps the Central Dome, shearing associated with its displacement would have to have been significantly more localized. A lack of significant ultramafic rock in the Central Dome region would be expected to play an important role in such difference. Some strain may also have partitioned into breccia zones within the gabbro, the thickness of which may be underestimated due to poor recovery and overprinting by undeformed diabase/basalt intrusions. Con-

straints on the thickness of detachment-related deformation across the southeast shoulder are currently lacking.

[62] Published tomographic models of refractions recorded on the MCS streamer also document along-strike variability within the domal core. *Canales et al.* [2008] show that shallow compressional wave velocities are generally high (5.5–6.5 km/s) in the middle and eastern flank of the Central Dome, and gradients in the upper few hundred meters exceed that of average young Atlantic crust [*White et al.*, 1992] (compare curves to gray shaded region in Figure 3e). In comparison, the central section of the Southern Ridge, where MCS Line 4 crosses (location in Figure 2), has gradients in the upper km that are typical of young Atlantic crust and velocity is lower (3.5–4.5 km/s; Figures 3d–3e). This part of the Southern Ridge has shallow velocity structure similar to the western flank of the Central Dome. Geologic mapping, geochemistry and these seismic results led to a previously proposed model that predicts the Southern Ridge consists dominantly of altered ultramafic rocks in contrast to the mafic-dominated Central Dome [*Karson et al.*, 2006; *Canales et al.*, 2008]. The few km scale of shallow velocity variability observed within Atlantis Massif is similar to what has been documented in the upper ~1 km at the Kane OCC [*Xu et al.*, 2009].

[63] While along-strike heterogeneity clearly exists within the footwall of the Atlantis Massif OCC, additional seismic analysis shows that significant cross-strike heterogeneity also occurs within the Southern Ridge. New tomographic results for MCS Line 9 [*Henig et al.*, 2009], which crosses the entire Southern Ridge (Figure 2), and had not previously been studied in detail, indicate that the southeast shoulder may be more similar to the Central Dome. High seismic velocity and steep gradients at shallow depths characterize this area; velocity-depth profiles for the southeast shoulder portion of Henig's tomography model plot with the solid curves for Lines 10 and 4 in Figure 3e.

[64] The Southern Ridge has a doubly plunging corrugated surface, although the south dipping portion only exists on the southeast shoulder today (Figure 2). Presumably the extension of this surface to the south of the present-day peak of the massif, at the center of the Southern Ridge, has undergone mass wasting with the arcuate headwall scarps at the top of the South Wall demonstrating this process [*Blackman et al.*, 2002; *Karson et al.*, 2006]. Applying the structural projection of *Schroeder and John* [2004], all mapping and sampling to date on the Southern Ridge is located less than ~500 m below the paleodetachment. Thus, current understanding of the 3-D geometry of the detachment fault system is limited to the upper half kilometer in what is a multikm (vertical and lateral) tectonic feature. The upper section is unquestionably crucial for understanding the evolution of Atlantis Massif but our knowledge of the deeper levels of the core complex remains limited. While the seafloor dominance of serpentinized harzburgite at the top of the South Wall is certain, the subseafloor extent of this rock type is not yet proven. *Canales et al.*'s [2008] seismic interpretation that the central Southern Ridge is dominantly serpentinized peridotite is quite reasonable given the rock types exposed on the upper South Wall. However, it is also true that the velocity structure is typical of average young Atlantic crust (Figure 3e), which could point toward fractured mafic crust underlain by competent, mainly gabbroic lower crust. The model of *Ildefonse et al.* [2007a] raises the possibility that what has been sampled to date on the South Wall represents a sheath of deformed rock, dominantly altered peridotite, which surrounds gabbroic plutons at the core of the OCC. The recently recognized higher seismic velocities in the southeast shoulder [*Henig et al.*, 2009] may support such an inference. Geologic data on the eastern part of the Southern Ridge are sparse. Of 14 Alvin samples from dive 3647 there, two are talus samples of serpentinized peridotite and six each are gabbro and metabasalt [*Blackman et al.*, 2002]. A very large dredge haul containing only gabbro was recovered from further down the slope (Figure 2) [*Cann et al.*, 1997; *Blackman et al.*, 1998]. Towed video mapping on the northern flank of the southeast shoulder (location in Figure 2) imaged pillow basalt. Such observations can be viewed in support of the southeast shoulder being underlain dominantly by mafic rocks.

[65] Evidence for alternatives to the *Ildefonse et al.* [2007a] hypothesis also exists at Atlantis Massif. Beneath the deformed rock in the top 100 m of the Southern Ridge [*Schroeder and John*, 2004; *Karson et al.*, 2006], the bedrock includes a fair amount of little-deformed serpentinized peridotite. It is not just gabbro that avoided strong deformation as the domal core was unroofed. The seismic data alone cannot rule out the possibility that the increase in cross-strike velocity and gradient from central to eastern Southern Ridge is, in part, due to presence of less altered peridotite in the southeast. A small (+5–8 mGal) residual gravity anomaly remains after removal of a 3-D gabbroic core contribution from the Bouguer anomaly [*Blackman et al.*, 2008]. Occurrence of slightly altered peridotite could produce this signal, although presence of significant oxide gabbro at shallow depths could as well. Geochemical analysis of samples from the SE shoulder area was not conducted for the *Delacour et al.* [2008] or *Boschi et al.* [2006] studies; such work would shed light on how evolution of the Southern Ridge compares with that of the Central Dome.

7.2. Working Model for the Evolution of Atlantis Massif OCC

[66] The present drilling and regional results provide sufficient information to explore a model for the evolution of Atlantis Massif OCC (Figure 11). In addition to the basic geologic and geophysical constraints, we consider limits on the likely pressure/temperature of magma crystallization and temperatures/fluid:rock ratios of alteration experienced by the sequence as it cooled (sections 5.1, 5.4, Table 2). The tectonic elements in our model are guided by the observed deformation within the cored sequence (section 5.2), observations along the South Wall (section 7.1) and present-day seafloor morphology.

[67] To develop a tectonic framework for the evolution of Atlantis Massif we need some constraint on the slip history along the detachment. Pb/U zircon ages available from widely spaced samples along the South Wall, taken with the average age obtained for Hole U1309D, have been used to estimate a time-integrated slip rate for the detachment system of 28.7 ± 6.7 mm/yr for at least 200 kyr [*Grimes et al.*, 2008]. This rate is essentially the full spreading rate in this part of the MAR [*Pariso et al.*, 1996]. One possible model would have the detachment, inferred (on the basis that spreading parallel corrugations mark relative slip between the footwall and

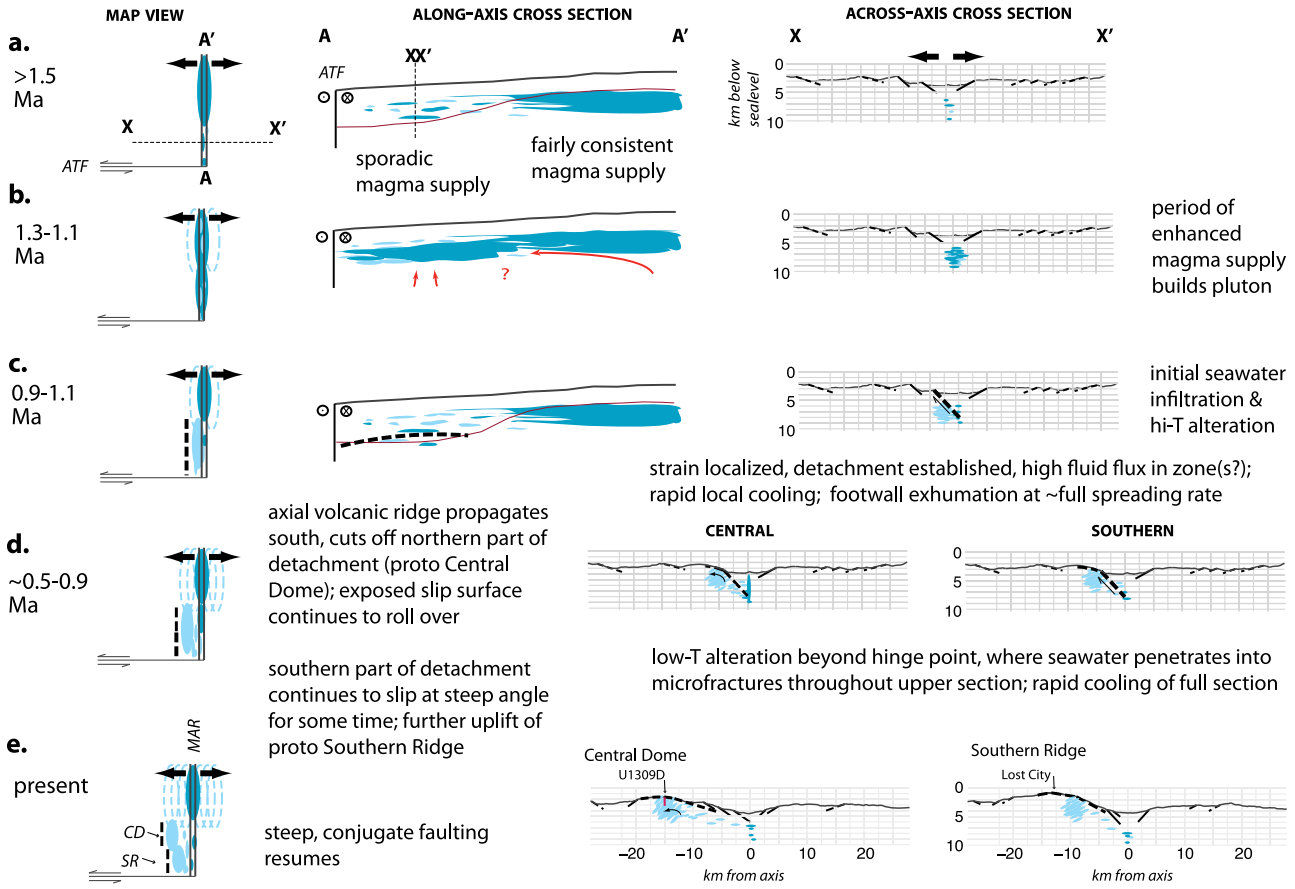

Figure 11. Working model for 3-D evolution of Atlantis Massif OCC. Thick dash shows active fault, thin dash shows inactive trace (in map view, line thickness relates to activity below seafloor, to east of surface trace shown). Dark blue indicates current magmatism; light blue indicates past intrusion.

hanging wall) to be exposed across the Central Dome, slipping at rates/times that coincide with activity on the detachment exposed on the Southern Ridge. Existing U/Pb zircon data are consistent with this interpretation, but do not require it. For this scenario to fit Atlantis Massif, the evolution of the two regions following the period when a detachment served as the main locus of plate separation must differ. Uplift of the Southern Ridge uplift was greater, and the western edge of the corrugated surface on the Central Dome is a few km farther west than where any striations or corrugations are evident on the Southern Ridge. (Figures 1c and 2).

[68] Prior to about 1.5 Ma, the ridge segment north of Atlantis Transform Fault (ATF) was likely typical for a slow-spreading ridge: consistent magma supply to the center of the segment and variable, often reduced supply within 15–20 km of the transform (Figure 11a).

[69] An episode of enhanced melt supply [*Ildefonse et al.*, 2007a] occurred ~1.1–1.3 Ma and magma was injected in the southern part of the segment (Figure 11b). These would become the rocks dated by *Grimes et al.* [2008], with ages possibly biased toward the end of the episode since late-stage oxide gabbro and felsic veins are the predominate rocks types hosting zircon.

[70] Steep faults at the seafloor propagated downward and connected with the weakened, altered (by magmatic fluids, minor seawater) [*Ildefonse et al.*, 2007a; *Jöns et al.*, 2009; *Nozaka and Fryer*, 2011] zone surrounding the new pluton. This throughgoing fault zone served as a conduit for seawater penetration to a significant depth (Figure 11c). Localization of strain occurred as alteration further weakened this zone and the detachment fault was established. High fluid flow rapidly cooled the detachment zone and relative plate motion focused mainly along it for at least 0.2 m.y., perhaps more. Fault slip resulted in westward offset and uplift of the footwall, with some initial rollover occurring due to nonzero flexural strength of the lithosphere. This bending opened (micro) fractures that allowed onset of static alteration in the upper few hundred meters as the footwall was exposed.

[71] Magmatism in the center of the segment presumably continued through the 1.5–1.1 Ma period and eventually an axial volcanic ridge propagated south into the early dome portion of the segment, cutting off activity on the northern part of the detachment (~0.9 Ma, Figure 11d). This is the scenario proposed by *MacLeod et al.* [2009] to typify the latter part of the 'life cycle' of an OCC. The paleoaxial volcanic ridge responsible for causing cessation of displacement along the northern part of the detachment at Atlantis Massif would be the one currently atop the eastern edge of the hanging wall block (Figures 1a and 1c). Hummocky backscatter pattern, many closed contour bathymetric

features capping the ridge, and its greater local relief compared to the low hummocks that cover most the hanging wall, all support the interpretation of the ridge as a volcanic chain, rather than just an upturned lip of the hanging wall block. This volcanic ridge is present along much of the hanging wall edge [*Blackman et al.*, 1998] but it does not extend completely along the Central Dome and certainly not to the Southern Ridge. Thus, we propose that the southern part of the detachment continued to slip for somewhat longer, contributing to the greater uplift of the Southern Ridge.

[72] While the southern footwall displacement ensued as a mix of detachment-controlled vertical and lateral motion, the central blocks experienced mostly horizontal motion and domino block rotation associated with en echelon steep faults, such as *Schroeder et al.* [2007] suggest to be the mode by which axial material transitions from vertical to lateral motion at a slow spread ridge with modest magma supply. Around 0.5 Ma, the southern detachment was cut by a younger, steeper fault and both central and southern domal highs became part of the relatively coherent lithosphere, rafting along with the overall motion of the western flank of the MAR (Figure 11e).

[73] There are aspects of Atlantis Massif that this model does not address. One is the western shoulder of the Southern Ridge. Sonar and a single video run there do not appear to provide conclusive indication of the rock type. Gravity analysis indicates that the overall density of this part of the Southern Ridge is somewhat lower than that of the middle and eastern parts [*Blackman et al.*, 2008] which, when taken with the bathymetry, might suggest this area is underlain by fractured basalt. The deeper video run on the western shoulder (Figure 2) imaged probable pillow basalts in a small graben where structure was more visible than immediate surroundings. However, the side scan signature of the top of the western shoulder, which was characterized as 'basement' by *Blackman et al.* [1998], is not typical of volcanic constructional seafloor. Our model for the history of slip on the detachment would not, in 2-D, explain why the western shoulder is as shallow as the rest of the Southern Ridge. If the transform is a relatively low-friction fault [*Fox and Gallo*, 1984], perhaps this allowed uplift of the older crust, outboard of the detachment, to occur whereas it was inhibited in the Central Dome region.

[74] Other models could also explain aspects of our current knowledge of Atlantis Massif. The interpretation of Henig's seismic results as a few km gabbroic body in the southeast shoulder could be explained by enhanced magmatic intrusion in that southernmost portion of the segment, which was not coeval with the intrusions that were drilled in the Central Dome. In this case, along-strike variation in the timing and duration of detachment faulting would be expected and would control how morphology of the Central Dome versus Southern Ridge developed. Lithology of the footwall would not necessarily be similar for the Central Dome and Southern Ridge. This type of model is favored for the Kane OCC [*Dick et al.*, 2008; *Xu et al.*, 2009]. In this scenario, the need for the transform to play a role in allowing enhanced uplift of the Southern Ridge is removed, since this dome evolves independent of the Central Dome. The steep scarp on the eastern side of the Southern Ridge could then represent a fault termination of this detachment. *Cannat et al.* [2009] note that steep scarps bound the young side of many OCC on the flanks of the southwest Indian ridge. They propose that these mark steep faults that terminate slip on the detachment system, as plate rigidity transitions from a period of localized weakness to generally greater strength.

[75] To test between the model we propose and others, comparison of the petrologic and geochemical signatures of the Central Dome and southeast shoulder gabbros is a worthwhile starting point that could begin immediately with existing samples. Additional subseafloor sampling would improve the strength of such investigation. Detailed comparison of the seismic properties within the Central Dome and Southern Ridge can also shed more light. The downward-continued MCS refraction data provide the most robust results throughout the interval covered, and comparison of different portions of the footwall is a component of work that is currently underway for Atlantis Massif [*Henig et al.*, 2009]. Future data that could test between models include oriented paleomagnetic samples across the Southern Ridge, to compare any rotation with that documented in the Central Dome. Our model predicts somewhat greater rotation of the former than the latter; the *Cannat et al.* [2009] model might predict less rotation for the Southern Ridge. Seismic velocity measurements of the lithosphere across the Southern Ridge and conjugate crust at 1.5–8 km depths would allow comparison of vertical and lateral structure to that obtained along an existing 40 km refraction profile across the Central Dome [*Blackman and Collins*, 2010].

8. Conclusions

[76] The results obtained through analysis of the IODP data from Atlantis Massif provided fundamental new insights on the formation and evolution of the oceanic core complex at this site. Some of the findings required that prior interpretations of the structure of Atlantis Massif be revised. In particular, the Central Dome was shown to be dominantly mafic, rather than ultramafic; more in-depth geophysical analyses were inspired and produced models that are consistent with this petrologic result. The geologic inferences available at the drill site can be extended using the regional survey data that also cover the Southern Ridge of the massif, where seafloor mapping is fairly extensive. With this along-strike view, it is clear that differences in the extents of magmatic intrusion along the axis and/or the timing and duration of detachment fault activity must have shaped the evolution of the massif. The working model that we put forth includes mechanisms for producing along/across strike variability that differ somewhat from prior models developed for the Kane [*Dick et al.*, 2008; *Xu et al.*, 2009] and 13°N MAR [*MacLeod et al.*, 2009] core complex regions; each of these models warrant further testing as additional data become available.

[77] The relatively continuous sampling with depth provided by the drill core was crucial for understanding the nature of magmatic intrusions that built the domal core at Atlantis Massif. High recovery enabled assessment of the extents and styles of alteration associated with fluid circulation as strain localized, the detachment fault formed, and the footwall was unroofed and exposed at the seafloor. The main findings from postcruise analysis of the IODP data are:

[78] 1. A series of magmatic intrusions formed the rocks recovered by drilling in the upper 1.4 km of the footwall to the exposed detachment fault. Preexisting mantle peridotites

were fluxed by melt and transformed into olivine-rich troctolites. Their volume in this part of the footwall is rather limited (a few percent of the total sequence).

[79] 2. Little deformation is recorded in the drill core and what occurs is quite localized. While brecciation and alteration patterns in the top 80 m may indicate a broader zone of shearing, rare schist fragments, inferred to mark the exposed detachment fault, were recovered but most were in the top few meters. Paleomagnetic data indicate that the footwall has tilted at least 45°, supporting a rolling hinge model for core complex development. Combined with the sparse and very localized deformation, this implies mainly coherent behavior of the footwall to a depth of 1.5 km minimum.

[80] 3. Seawater infiltration was pervasive in the upper ~380 m, with high fluid-rock ratios documented for the upper ~100 m. Alteration at greater depths is moderate and only occurs in local zones below 800 mbsf, mainly near veins and igneous contacts.

[81] **Acknowledgments.** This research used samples and data provided by the Integrated Ocean Drilling Program (IODP). The tomographic model in Figure 3d was kindly provided by Pablo Canales. We thank Jeff Karson for his thorough and insightful review; it helped us significantly improve the manuscript. An anonomous reviewer's comments on the alteration aspects helped us clarify and increase the synthesis of those results.

References

Bach, W., and F. Klein (2009), The petrology of seafloor rodingites: Insights from geochemical reaction path modeling, *Lithos*, *112*, 103–117, doi:10.1016/j.lithos.2008.10.022.

Beard, J. S., et al. (2009), Onset and progression of serpentinization and magnetite formation in olivine-rich troctolite from IODP Hole U1309D, *J. Petrol.*, *50*, 387–403, doi:10.1093/petrology/egp004.

Blackman, D. K., and J. A. Collins (2010), Lower crustal variability and the crust/mantle transition at the Atlantis Massif oceanic core complex, *Geophys. Res. Lett.*, *37*, L24303, doi:10.1029/2010GL045165.

Blackman, D. K., et al. (1998), Origin of extensional core complexes: Evidence from the Mid-Atlantic Ridge at Atlantis fracture zone, *J. Geophys. Res.*, *103*, 21,315–21,333, doi:10.1029/98JB01756.

Blackman, D. K., et al. (2002), Geology of the Atlantis Massif (MAR 30°N): Implications for the evolution of an ultramafic oceanic core complex, *Mar. Geophys. Res.*, *23*, 443–469, doi:10.1023/B:MARI.0000018232.14085.75.

Blackman, D. K., et al. (2004), Oceanic core complex formation, Atlantis Massif—Oceanic core complex formation, Atlantis Massif, Mid-Atlantic Ridge: Drilling into the footwall and hanging wall of a tectonic exposure of deep, young oceanic lithosphere to study deformation, alteration, and melt generation, *Integrated Ocean Drill. Program Sci. Prospectus, 304/305*, doi:10.2204/iodp.sp.304305.2004.

Blackman, D. K., B. Ildefonse, B. E. John, Y. Ohara, D. J. Miller, and C. J. MacLeod, and the Expedition 304/305 Scientists (2006) *Proceedings of the Integrated Ocean Drilling Program*, vol. 304/305, Integrated Ocean Drilling Program, College Station, Tex., doi:10.2204/iodp.proc.304305.2006.

Blackman, D. K., et al. (2008), Three-dimensional structure of oceanic core complexes: Effects on gravity signature and ridge flank morphology, Mid-Atlantic Ridge 30°N, *Geochem. Geophys. Geosyst.*, *9*, Q06007, doi:10.1029/2008GC001951.

Blackman, D. K., et al. (2009), Geophysical signatures of oceanic core complexes, *Geophys. J. Int.*, *178*, 593–613, doi:10.1111/j.1365-246X.2009.04184.x.

Bonatti, E., and J. Honnorez (1976), Sections of the Earth's crust in the equatorial Atlantic, *J. Geophys. Res.*, *81*, 4104–4116, doi:10.1029/JB081i023p04104.

Boschi, C., et al. (2006), Mass transfer and fluid flow during detachment faulting and development of an oceanic core complex, Atlantis Massif (MAR 30°N), *Geochem. Geophys. Geosyst.*, *7*, Q01004, doi:10.1029/2005GC001074.

Buck, W. R. (1988), Flexural rotation of normal faults, *Tectonics*, *7*, 959–973, doi:10.1029/TC007i005p00959.

Buck, W. R., et al. (2005), Modes of faulting at mid-ocean ridges, *Nature*, *434*, 719–723, doi:10.1038/nature03358.

Canales, J. P., et al. (2004), Seismic reflection imaging of an oceanic detachment fault: Atlantis megamullion (Mid-Atlantic Ridge, 30°10′ N), *Earth Planet. Sci. Lett.*, *222*, 543–560, doi:10.1016/j.epsl.2004.02.023.

Canales, J. P., et al. (2008), Seismic evidence for large-scale compositional heterogeneity of oceanic core complexes, *Geochem. Geophys. Geosyst.*, *9*, Q08002, doi:10.1029/2008GC002009.

Cann, J. R., et al. (1997), Corrugated slip surfaces formed at ridge-transform intersections on the Mid-Atlantic Ridge, *Nature*, *385*, 329–332, doi:10.1038/385329a0.

Cannat, M. (1993), Emplacement of mantle rock in the seafloor at mid-ocean ridges, *J. Geophys. Res.*, *98*, 4163–4172, doi:10.1029/92JB02221.

Cannat, M., et al. (1997), Ultramafic and gabbroic exposures at the Mid-Atlantic Ridge: Geological mapping in the 15° N region, *Tectonophysics*, *279*, 193–213, doi:10.1016/S0040-1951(97)00113-3.

Cannat, M., et al. (2009), Oceanic corrugated surfaces and the strength of the axial lithosphere at slow spreading ridges, *Earth Planet. Sci. Lett.*, *288*, 174–183, doi:10.1016/j.epsl.2009.09.020.

Collins, J., et al. (2003), Seismic velocity structure of mid-Atlantic ridge core complexes, *Geophys. Res. Abstr.*, *5*, EAE03-A-10390.

Collins, J. A., et al. (2009), Seismic and drilling constraints on velocity structure and reflectivity near IODP Hole U1309D on the Central Dome of Atlantis Massif, Mid-Atlantic Ridge 30°N, *Geochem. Geophys. Geosyst.*, *10*, Q01010, doi:10.1029/2008GC002121.

Delacour, A., et al. (2008), Sr- and Nd-isotope geochemistry of the Atlantis Massif (30°N, MAR): Implications for fluid fluxes and lithospheric heterogeneity, *Chem. Geol.*, *254*, 19–35, doi:10.1016/j.chemgeo.2008.05.018.

Dick, H. J. B. (1989), Abyssal peridotites, very slow spreading ridges and ocean ridge magmatism, in *Magmatism in the Ocean Basins*, edited by A. D. Saunders and M. J. Norry, pp. 71–105, Geol. Soc., London, doi:10.1144/GSL.SP.1989.042.01.06.

Dick, H. J. B., et al. (2000), A long in situ section of lower ocean crust: Results of ODP Leg 176 drilling at the southwest Indian Ridge, *Earth Planet. Sci. Lett.*, *179*, 31–51. doi:10.1016/S0012-821X(00)00102-3.

Dick, H. J. B., et al. (2008), Plutonic foundation of a slow-spreading ridge segment: The oceanic core complex at Kane Megamullion, 23°30′N, 45°20′W, *Geochem. Geophys. Geosyst.*, *9*, Q05014, doi:10.1029/2007GC001645.

Drouin, M., et al. (2007), Origin of olivine-rich troctolites from IODP Hole U1309D in the Atlantis Massif (Mid-Atlantic Ridge): Petrostructural and geochemical study, *Eos Trans. AGU*, *88*(52), Fall Meet. Suppl., Abstract T53B–1300.

Drouin, M., et al. (2009), In situ geochemistry of olivine-rich troctolites (IODP Hole U1309D, Atlantis Massif, Mid-Atlantic Ridge, 30°N): A record of magmatic impregnation in the lower oceanic crust, *Chem. Geol.*, *264*, 71–88, doi:10.1016/j.chemgeo.2009.02.013.

Drouin, M., et al. (2010), A microstructural imprint of melt impregnation in slow spreading lithosphere: Olivine-rich troctolites from the Atlantis Massif, Mid-Atlantic Ridge, 30°N, IODP Hole U1309D, *Geochem. Geophys. Geosyst.*, *11*, Q06003, doi:10.1029/2009GC002995.

Escartín, J., et al. (2001), Strength of slightly serpentinized peridotites: Implications for the tectonics of oceanic lithosphere, *Geology*, *29*, 1023–1026, doi:10.1130/0091-7613(2001)029<1023:SOSSPI>2.0.CO;2.

Escartín, J., et al. (2003), Constraints on deformation conditions and the origin of oceanic detachments, the Mid-Atlantic Ridge core complex at 15°45′N, *Geochem. Geophys. Geosyst.*, *4*(8), 1067, doi:10.1029/2002GC000472.

Fox, P. J., and D. G. Gallo (1984), A tectonic model for ridge-transform ridge plate boundaries: Implications for the structure of oceanic lithosphere, *Tectonophysics*, *104*, 205–242, doi:10.1016/0040-1951(84)90124-0.

Frost, B. R., et al. (2008), The formation of microrodingites from IODP Hole U1309D: Key to understanding the process of serpentinization, *J. Petrol.*, *49*, 1579–1588, doi:10.1093/petrology/egn038.

Früh-Green, G. L., et al. (2003), 30,000 years of hydrothermal activity at the Lost City vent field, *Science*, *301*, 495–498, doi:10.1126/science.1085582.

Garcés, M., and J. S. Gee (2007), Paleomagnetic evidence of large footwall rotations associated with low-angle faults at the Mid-Atlantic Ridge, *Geology*, *35*, 279–282, doi:10.1130/G23165A.1.

Godard, M., et al. (2009), Geochemistry of long in-situ section of intrusive slow spread oceanic lithosphere: Results from IODP Site 1309, *Earth Planet. Sci. Lett.*, *279*, 110–122, doi:10.1016/j.epsl.2008.12.034.

Grimes, C. B., et al. (2008), Protracted construction of gabbroic crust at a slow spreading ridge: Constraints from $^{206}Pb/^{238}U$ zircon ages from Atlantis Massif and IODP Hole U1309D (30°N, MAR), *Geochem. Geophys. Geosyst.*, *9*, Q08012, doi:10.1029/2008GC002063.

Grimes, C. B., et al. (2011), Cooling rates and the depth of detachment faulting at oceanic core complexes: Evidence from zircon Pb/U and U-Th/He ages, *Geochem. Geophys. Geosyst.*, *12*, Q0AG01, doi:10.1029/2010GC003391.

Harding, A. J., et al. (2007), A new method for MCS refraction data analysis of the uppermost section at a Mid-Atlantic Ridge core complex, *Eos Trans. AGU*, *88*(52), Fall Meet. Suppl., Abstract S12A–03.

Henig, A. S., et al. (2009), Seismic velocity variation within the footwall of an oceanic core complex: Atlantis Massif, Mid-Atlantic Ridge 30°N, *InterRidge Newsl.*, *18*, 9–13. (Available at http://www.interridge.org/IRNewsletter).

Hirose, T., and N. W. Hayman (2008), Structure, permeability, and strength of a fault zone in the footwall of an oceanic core complex, the Central Dome of the Atlantis Massif, Mid-Atlantic Ridge, 30°N, *J. Struct. Geol.*, *30*, 1060–1071, doi:10.1016/j.jsg.2008.04.009.

Ildefonse, B., et al. (2007a), Oceanic core complexes and crustal accretion at slow-spreading ridges, *Geology*, *35*, 623–626, doi:10.1130/G23531A.1.

Ildefonse, B., et al. (2007b), Deep sampling of the crust formed at Mid-Ocean Ridges: Scientific ocean drilling provides 'in-depth' perspective, *Oceanography*, *20*, 22–33.

John, B. E. (1987), Geometry and evolution of a mid-crustal extensional fault system: Chemehuevi Mountains, southeastern California, *Spec. Pap. Geol. Soc. London*, *28*, 313–335.

John, B. E., and M. J. Cheadle (2010), Deformation and alteration associated with oceanic and continental detachment fault systems: Are they similar? in *Diversity of Hydrothermal Systems on Slow Spreading Ocean Ridges*, *Geophys. Monogr. Ser*, vol. 188, edited by P. Rona, et al., pp. 175–206, AGU, Washington, D. C.

John, B. E., et al. (2009), Data report: Spatial and temporal evolution of slow spread oceanic crust—Graphic sections of core recovered from IODP Hole U1309D, Atlantis Massif, 30°N, MAR (including Pb/U zircon geochronology and magnetic remanence data), in *Proceedings of the Integrated Ocean Drilling Program*, vol. 304/305, edited by D. K. Blackman et al., Integrated Ocean Drilling Program, College Station, Tex., doi:10.2204/iodp.proc.304305.205.2009.

Jöns, N., W. Bach, and T. Schroeder (2009), Formation and alteration of plagiogranites in an ultramafic-hosted detachment fault at the Mid-Atlantic Ridge (ODP Leg 209), *Contrib. Mineral. Petrol.*, *157*, 625–639, doi:10.1007/s00410-008-0357-2.

Karson, J. A. (1990), Seafloor spreading on the Mid-Atlantic Ridge: Implications for the structure of ophiolites and oceanic lithosphere produced in slow-spreading environments, in *Proceedings of Symposium Troodos 1987*, edited by J. Malpas, pp. 547–553, Geol. Surv. Dep., Nicosia.

Karson, J. A., and D. Elthon (1987), Evidence for variations in magma production along ocanic spreading centers: A critical appraisal, *Geology*, *15*, 127–131, doi:10.1130/0091-7613(1987)15<127:EFVIMP>2.0.CO;2.

Karson, J. A., et al. (1984), The geology of the Oceanography transform: The ridge-transform intersections, *Mar. Geophys. Res.*, *6*, 109–141, doi:10.1007/BF00285956.

Karson, J. A., et al. (1997), *Proceedings of the Ocean Drilling Program Scientific Results*, vol. 153, Ocean Drilling Program, College Station, Tex.

Karson, J. A., et al. (2006), Detachment shear zone of the Atlantis Massif core complex, Mid-Atlantic Ridge, 30°N, *Geochem. Geophys. Geosyst.*, *7*, Q06016, doi:10.1029/2005GC001109.

Kelemen, P. B., et al. (2007), Leg 209 summary: Processes in a 20-km-thick conductive boundary layer beneath the Mid-Atlantic Ridge, 14°–16°N, *Proc. Ocean Drill. Program, Sci. Results*, *209*, 1–33. doi:10.2973/odp.proc.sr.209.001.2007.

Kelley, D. S., et al. (2001), An off-axis hydrothermal vent field discovered near the Mid-Atlantic Ridge at 30°N, *Nature*, *412*, 145–149, doi:10.1038/35084000.

Lagabrielle, Y., et al. (1998), Ultramafic-mafic plutonic rock suites exposed along the Mid-Atlantic Ridge (10°N–30°N): Symmetrical-asymmetrical distribution and implications for seafloor spreading processes, in *Faulting and Magmatism at Mid-Ocean Ridges*, edited by W. R. Buck, J. A. Karson, and Y. Lagabrielle, pp. 153–176, AGU, Washington, D. C.

Lin, J., et al. (1990), Evidence from gravity data for focused magmatic accretion along the Mid-Atlantic Ridge, *Nature*, *344*, 627–632, doi:10.1038/344627a0.

Lissenberg, C. J., and H. J. B. Dick (2008), Melt-rock reaction in the lower oceanic crust and its implications for the genesis of mid-ocean ridge basalt, *Earth Planet. Sci. Lett.*, *271*, 311–325, doi:10.1016/j.epsl.2008.04.023.

MacLeod, C. J., et al. (2002), Direct geological evidence for oceanic detachment faulting: The Mid-Atlantic Ridge, 15, *Geology*, *30*, 879–882, doi:10.1130/0091-7613(2002)030<0879:DGEFOD>2.0.CO;2.

MacLeod, C. J., et al. (2009), LIfe cycle of oceanic core complexes, *Earth Planet. Sci. Lett.*, *287*, 333–344, doi:10.1016/j.epsl.2009.08.016.

McCaig, A. M., et al. (2007), Oceanic detachment faults focus very large volumes of black smoker fluids, *Geology*, *35*, 935–938, doi:10.1130/G23657A.1.

McCaig, A. M., et al. (2010), Detachment fault control on hydrothermal circulation systems: Interpreting the subsurface beneath the TAG hydrothermal field using the isotopic and geological evolution of oceanic core complexes in the Atlantic, in *Diversity of Hydrothermal Systems on Slow Spreading Ocean Ridges*, *Geophys. Monogr. Ser.*, vol. 188, edited by P. Rona et al., pp. 207–240, AGU, Washington, D. C.

Mehl, L., and G. Hirth (2008), Plagioclase preferred orientation in layered mylonites: Evaluation of flow laws for the lower crust, *J. Geophys. Res.*, *113*, B05202, doi:10.1029/2007JB005075.

Michibayashi, K., et al. (2008), Hydration due to high-T brittle failure within in situ oceanic crust, 30°N Mid-Atlantic Ridge, *Earth Planet. Sci. Lett.*, *275*, 348–354, doi:10.1016/j.epsl.2008.08.033.

Minshull, T. A., et al. (1998), Is the oceanic Moho a serpentinization front?, in *Modern Ocean Floor Processes and the Geological Record*, pp. 71–80, Geol. Soc., London, doi:10.1144/GSL.SP.1998.148.01.05.

Miranda, E. A., and Y. Dilek (2010), Oceanic core complex development in modern and ancient oceanic lithosphere: Gabbro-localized versus peridotite-localized detachment models, *J. Geol.*, *118*, 95–109, doi:10.1086/648460.

Miranda, E. A., and B. E. John (2010), Strain localization along the Atlantis Bank oceanic detachment fault system, southwest Indian Ridge, *Geochem. Geophys. Geosyst.*, *11*, Q04002, doi:10.1029/2009GC002646.

Morris, A., et al. (2009), Footwall rotation in an oceanic core complex quantified using reoriented Integrated Ocean Drilling Program core samples, *Earth Planet. Sci. Lett.*, *287*, 217–228, doi:10.1016/j.epsl.2009.08.007.

Nooner, S. L., et al. (2003), Constraints on crustal structure at the Mid-Atlantic Ridge from seafloor gravity measurements made at the Atlantis Massif, *Geophys. Res. Lett.*, *30*(8), 1446, doi:10.1029/2003GL017126.

Nozaka, T., and P. Fryer (2011), Alteration of he oceanic lower crust at a slow-spreading axis: Insight from vein-related zoned halos in olivine gabbro from Atlantis Massif, Mid-Atlantic Ridge, *J. Petrol.*, *52*, 643–664, doi:10.1093/petrology/egq098.

Nozaka, T., et al. (2008), Formation of clay minerals and exhumation of lower-crustal rocks at Atlantis Massif, Mid-Atlantic Ridge, *Geochem. Geophys. Geosyst.*, *9*, Q11005, doi:10.1029/2008GC002207.

Ohara, Y., et al. (2007), Seismic study on oceanic core complexes in the Parece Vela back-arc basin, *Isl. Arc*, *16*, 348–360, doi:10.1111/j.1440-1738.2007.00591.x.

Pariso, J. E., et al. (1996), Three-dimensional inversion of marine magnetic anomalies: Implications for crustal accretion along the Mid-Atlantic Ridge (28°–31°30′N), *Mar. Geophys. Res.*, *18*, 85–101, doi:10.1007/BF00286204.

Schouten, H., D. K. Smith, J. R. Cann, and J. Escartín (2010), Tectonic versus magmatic extension in the presence of core complexes at slow-spreading ridges from a visualization of faulted seafloor topography, *Geology*, *38*, 615–618, doi:10.1130/G30803.1.

Schroeder, T., and B. E. John (2004), Strain localization on an oceanic detachment fault system, Atlantis Massif, 30°N, Mid-Atlantic Ridge, *Geochem. Geophys. Geosyst.*, *5*, Q11007, doi:10.1029/2004GC000728.

Schroeder, T., et al. (2007), Nonvolcanic seafloor spreading and corner-flow rotation accommodated by extensional faulting at 15°N on the Mid-Atlantic Ridge: A structural synthesis of ODP Leg 209, *Geochem. Geophys. Geosyst.*, *8*, Q06015, doi:10.1029/2006GC001567.

Singh, S. C., et al. (2004), New insights into serpentinization at Atlantis Massif, *Eos Trans. AGU*, *85*(47), Fall Meet. Suppl., Abstract V23B–0628.

Sinton, J. M., and R. S. Detrick (1992), Mid-ocean ridge magma chambers, *J. Geophys. Res.*, *97*, 197–216, doi:10.1029/91JB02508.

Smith, D. K., J. Escartín, H. Schouten, and J. R. Cann (2008), Fault rotation and core complex formation: Significant processes in seafloor formation at slow-spreading Mid-Ocean Ridges (Mid-Atlantic Ridge, 13–15 N), *Geochem. Geophys. Geosyst.*, *9*, Q03003, doi:10.1029/2007GC001699.

Suhr, G., et al. (2008), Stacked gabbro units and intervening mantle: A detailed look at a section of IODP Leg 305, Hole 1309D, *Geochem. Geophys. Geosyst.*, *9*, Q10007, doi:10.1029/2008GC002012.

Tamura, A., et al. (2008), Petrology and geochemistry of peridotites from IODP Site U1309 at Atlantis Massif, MAR 30°N: Micro- and macro-scale melt penetrations into peridotites, *Contrib. Mineral. Petrol.*, *155*, 491–509, doi:10.1007/s00410-007-0254-0.

Tucholke, B. E., and J. Lin (1994), A geological model for the structure of ridge segments in slow spreading ocean crust, *J. Geophys. Res.*, *99*, 11,937–11,958, doi:10.1029/94JB00338.

Tucholke, B. E., et al. (1998), Megamullions and mullion structure defining oceanic metamorphic core complexes on the Mid-Atlantic ridge, *J. Geophys. Res.*, *103*, 9857–9866, doi:10.1029/98JB00167.

Tucholke, B. E., et al. (2008), Role of melt supply in oceanic detachment faulting and formation of megamullions, *Geology*, *36*, 455–458, doi:10.1130/G24639A.1.

von der Handt, A., and E. Hellebrand (2010), Transformation of mantle to lower crust: Melt-rock reaction processes in peridotites from Atlantis

Massif, 30°N Mid-Atlantic Ridge, Abstract V11A–2244 presented at 2010 Fall Meeting, AGU, San Francisco, Calif. 13–17 Dec.

Wernicke, B., and G. J. Axen (1988), On the role of isostasy in the evolution of normal fault systems, *Geology*, *16*, 848–851, doi:10.1130/0091-7613(1988)016<0848:OTROII>2.3.CO;2.

White, R. S., et al. (1992), Oceanic crustal thickness from seismic measurements and rare earth element inversions, *J. Geophys. Res.*, *97*, 19,683–19,715, doi:10.1029/92JB01749.

Xu, M., et al. (2009), Heterogeneous seismic velocity structure of the upper lithosphere at Kane oceanic core complex, Mid-Atlantic Ridge, *Geochem. Geophys. Geosyst.*, *10*, Q10001, doi:10.1029/2009GC002586.

Zhao, X., and M. Tominaga (2009), Paleomagnetic and rock magnetic results from lower crustal rocks of IODP Site U1309: Implication for thermal and accretion history of the Atlantis Massif, *Tectonophysics*, *474*, 435–448, doi:10.1016/j.tecto.2009.04.017.

N. Abe, IFREE, JAMSTEC, Yokosuka, Kanagawa, 237-0061, Japan.

M. Abratis, Institute of Geosciences-Mineralogy, Friedrich Schiller University of Jena, D-07749 Jena, Germany.

E. S. Andal, Philex Mining Corporation, 27 Brixton St., Pasig City, 1600, Philippines.

M. Andreani, Laboratoire de Géologie, Université Claude Bernard Lyon 1, F-69622 Villeurbanne, CEDEX, France.

S. Awaji, Department of Geosystem Engineering, University of Tokyo, Tokyo, 113-8656, Japan.

J. S. Beard, Virginia Museum of Natural History, Martinsville, VA 24112, USA.

D. K. Blackman and J. S. Gee, Scripps Institution of Oceanography, University of California, San Diego, La Jolla, CA 92093, USA. (dblackman@ucsd.edu)

D. Brunelli, Dipartimento di Scienze della Terra, Universita Modena, I-41100 Modena, Italy.

A. B. Charney, Department of Geosciences, Oregon State University, Corvalis, OR 97331, USA.

D. M. Christie, Department of Fisheries and Ocean Sciences, University of Alaska Fairbanks, Fairbanks, AK 99775, USA.

J. Collins and M. Tominaga, Department of Marine Geology and Geophysics, Woods Hole Oceanographic Institution, Woods Hole, MA 02543, USA.

A. G. Delacour, Laboratoire de Dynamique Terrestre Planétaire, Université Toulouse, F-31400 Toulouse, France.

H. Delius, Department of Geology, University of Leicester, Leicester LE1 7RH, UK.

M. Drouin, Laboratoire Geosciences, Université Réunion, F-97716 Saint-Denis, CEDEX 9, France.

F. Einaudi, M. Godard, and B. Ildefonse, Géosciences Department, Université Montpellier 2, F-34095 Montpellier, CEDEX 5, France.

J. Escartín, Groupe de Geosciences Marines, Institut de Physique du Globe, F-75252 Paris, France.

B. R. Frost and B. E. John, Department of Geology and Geophysics, University of Wyoming, Laramie, WY 82071, USA.

G. Früh-Green, Department of Earth Sciences, ETH Zurich, CH-8092 Zurich, Switzerland.

P. B. Fryer, E. Hellebrand, and K. T. M. Johnson, School of Ocean and Earth Science and Technology, University of Hawaii at Manoa, Honolulu, HI 96822, USA.

C. B. Grimes, Department of Geosciences, Mississippi State University, Mississippi State, MS 39762, USA.

A. Halfpenny, Research School of Earth Sciences, Australian National University, Canberra, ACT 0200, Australia.

H.-E. Hansen, Department of Earth Science, University of Bergen, N-5020 Bergen, Norway.

A. C. Harris, Department of Geology and Environmental Sciences, Norwich University, Northfield, VT 05663, USA.

S. Ishimaru and A. Tamura, Department of Earth and Environmental Sciences, Kanazawa University, Kanazawa, 920-1102, Japan.

N. W. Hayman, Institute of Geophysics, University of Texas at Austin, Austin, TX 78758, USA.

T. Hirose, Kochi Institute for Core Sample Research, JAMSTEC, 200 Monobe Otsu, Nankoku City, Kochi, 783-8502, Japan.

J. G. Hirth, Department of Geological Sciences, Brown University, Providence, RI 02912, USA.

G. D. Karner, Exxon-Mobile URC, PO Box 2189, Houston, TX 77251, USA.

M. Linek, Baker Hughes, 2929 Allen Pkwy., Ste. 2100, Houston, TX 77019, USA.

C. J. MacLeod, Department of Earth and Ocean Sciences, Cardiff University, Cardiff, CF10 3YE, UK.

J. Maeda and T. Yamasaki, Department of Earth and Planetary Sciences, Hokkaido University, Sapporo, 060-0810, Japan.

O. U. Mason, Ecology Department, Lawrence Berkeley National Laboratory, 1 Cyclotron Rd., MS 90-1116, Berkeley, CA 94720, USA.

A. M. McCaig, Department of Earth Sciences, University of Leeds, Leeds LS2 9JT, UK.

K. Michibayashi, Institute of Geosciences, Shizuoka University, Shizuoka, 422-8529, Japan.

D. J. Miller, Integrated Ocean Drilling Program, Texas A&M University, College Station, TX 77845, USA.

A. Morris, Department of Earth and Environmental Sciences, University of Plymouth, Plymouth PL4 8AA, UK.

T. Nakagawa, Department of Chemical and Life Sciences, Nihon University, Fujisawa, Kanagawa, 252-8510, Japan.

T. Nozaka, Department of Earth Sciences, Okayama University, Okayama, 700-8530, Japan.

Y. Ohara, Hydrographic and Oceanographic Department, Ocean Research Laboratory, Tokyo, 104-0045, Japan.

M. Rosner, Mineral Properties and Transport Processes, GFZ, D-14473 Potsdam, Germany.

R. C. Searle, Department of Earth Sciences, Durham University, Durham DH1 3LE, UK.

G. Suhr, Institut für Geologie und Mineralogie, Universitat zu Köln, D-50674 Köln, Germany.

A. von der Handt, Department of Geosciences, University of Freiburg, D-79098 Freiburg, Germany.

X. Zhao, Department of Earth Sciences, University of California, Santa Cruz, CA 95064, USA.